A&A 372, 29–49 (2001)
DOI: 10.1051/0004-6361:20010439

Astronomy & Astrophysics

1.65 μm (H-band) surface photometry of galaxies

VII. Dwarf galaxies in the Virgo Cluster⋆

G. Gavazzi[1], S. Zibetti[1], A. Boselli[2], P. Franzetti[1], M. Scodeggio[3], and S. Martocchi[1]

[1] Università degli Studi di Milano–Bicocca, P.zza dell'Ateneo Nuovo 1, 20126 Milano, Italy
[2] Institut d'Astrophysique de Marseille, Traverse du Siphon, 13376 Marseille Cedex 12, France
[3] Istituto di Fisica Cosmica "G. Occhialini", CNR, via Bassini 15, 20133 Milano, Italy

Received 21 December 2000 / Accepted 21 March 2001

Abstract. We present near-infrared H-band (1.65 μm) observations and surface brightness profile decompositions for 75 faint ($13.5 \lesssim m_{\rm p} \lesssim 18.5$) galaxies, primarily taken among dwarf Ellipticals members of the Virgo cluster, with some Centaurus Cluster members, a BCD and two peculiar galaxies taken as fillers. We model their surface brightness profiles with a de Vaucouleurs (D), exponential (E), mixed (bulge+disk or M) or truncated (T) law, and we derive for each galaxy the H band effective surface brightness ($\mu_{\rm e}$) and effective radius ($r_{\rm e}$), the asymptotic total magnitude $H_{\rm T}$ and the light concentration index C_{31}, defined as the ratio between the radii that enclose 75% and 25% of the total light $H_{\rm T}$. For a subsample we compare the NIR surface photometry with similar data taken in the B and V bands, and we give the $B-H$ and $B-V$ color profiles. Combining the present data with those previously obtained by our group (1157 objects) we analyze the NIR properties of a nearly complete sample, representative of galaxies of all morphological types, spanning 4 decades in luminosity. We confirm our earlier claim that the presence of cusps and extended haloes in the light profiles ($C_{31} > 5$) is a strong, non-linear function of the total luminosity. We also find that: i) among dE and dS0 galaxies D profiles are absent; 50% of the decompositions are of type M, the remaining being of type E or T. ii) Less than 50% of the giant elliptical galaxies have pure D profiles, the majority being represented by M profiles. iii) Most giant galaxies (from elliptical to Sb) have M profiles. iv) Most of late type spirals (Scd to BCD) have either E or T profiles. v) The type of decomposition is a strong function of the total H band luminosity, independent of the Hubble classification: the fraction of type E decompositions decreases with increasing luminosity, while those of type M increase with luminosity. Pure D profiles are absent in the low luminosity range $L_{\rm H} < 10^{10}\ L_{\odot}$ and become dominant above $10^{11}\ L_{\odot}$, while T profiles are present only among low luminosity galaxies. vi) We find that dE-peculiar galaxies have structural parameters indistinguishable from those of late-type dwarfs, thus they might represent the missing link between dEs and dIs.

Key words. galaxies: fundamental parameters – galaxies: photometry – infrared: galaxies

1. Introduction

The comprehension of the physical processes behind the formation and evolution of galaxies is far from satisfactory, but plausible scenarios based on hierarchical clustering (Kauffmann & White 1993; Kauffmann & Charlot 1998), developed in the framework of CDM cosmology, are becoming the current paradigm superseeding previous models based on the monolithic collapse scenario (Larson 1975; Sandage 1986).

The advent of 8 m-class telescopes and of the forthcoming NGST will soon make it possible to trace observationally the evolution of galaxies up to redshifts of cosmological relevance, and therefore allow a direct comparison between model predictions and observations.

Should however adult galaxies retain some memory of their "infancy", observations carried out at $z = 0$ would provide important constraints on their evolutionary history. For these nearby objects even the present instrumentation is suitable for extending to intrinsically low luminosity galaxies a detailed determination of their "shape" and "size" parameters, such as color, morphology, and

Send offprint requests to: G. Gavazzi,
e-mail: Giuseppe.Gavazzi@mib.infn.it

⋆ Based on observations taken with the ESO/NTT (ESO program 64.N-0288), with the Telescopio Nazionale Galileo (TNG) operated on the island of La Palma by the Centro Galileo Galilei of the CNAA at the Spanish Observatorio del Roque de los Muchachos of the IAC, with the San Pedro Martir 2.1 m telescope of the Observatorio Astronomico Nacional (OAN, Mexico), and with the OHP 1.2 m telescope, operated by the French CNRS.

brightness profile, or luminosity, radius, and mass, respectively (see Whitmore 1984). These parameters are the constituents of the well known scaling relations of local galaxies: the Fundamental Plane for the Ellipticals (Djorgovski & Davis 1987; Dressler et al. 1987), and the Tully-Fisher relation for the Spiral galaxies (Tully & Fisher 1977).

Over the last two decades we have witnessed an extensive effort in studying these properties, limited however mostly to the optical bands. Less systematic efforts were devoted to Near infrared (NIR) investigations, in spite of these being the most suitable ones for studying the properties of galaxies, because most of a galaxy luminous mass sits in the old stellar population traced by NIR light (Gavazzi et al. 1996c), and because of the greatly reduced dust obscuration at these wavelengths. To fully exploit these two advantages we have made extensive use of NIR panoramic detectors to obtain H (and K') band images of nearby galaxies. We first concentrated on disk galaxies (see Gavazzi et al. 1996a, Paper I; Gavazzi et al. 1996b, Paper II; Boselli et al. 2000, Paper IV; Boselli et al. 1997 (B97)), while later we extended the survey to the early-types (Gavazzi et al. 2000a, Paper III). Using these data Gavazzi et al. (2000b, Paper V) studied the structural properties of galaxies that can be derived from surface-photometry measurements at NIR pass-bands: i.e. their light profiles. The observing sample was selected among members of 5 nearby, rich clusters: namely the Virgo, Coma, A1367, A262 and Cancer clusters, in addition to a significant population of galaxies in the "Great Wall", the bridge between Coma and A1367. The survey included a representative sample of galaxies spanning all morphological types (including Im and BCDs), except early-type dwarfs (dE, dS0) which were severely undersampled because, due to the their low surface brightness at NIR bandpasses, they could not be observed with 2 m class telescopes. Beside our work, early panoramic NIR observations exist for only 15 dwarf elliptical galaxies in the Virgo cluster, as reported by James (1991, 1994).

To fill this gap, we have obtained NIR imaging observations of 50 dwarf elliptical and dwarf S0 galaxies, of 11 dI galaxies and of 11 giant galaxies from the Virgo Cluster Catalogue (hereafter VCC, Binggeli et al. 1985) and from the Centaurus Cluster Catalogue (hereafter CCC, Jerjen & Dressler 1997). From these observations we derive the azimuthally averaged light profiles, that are fitted using either a de Vaucouleurs $r^{1/4}$ law, an exponential law, a mixed (bulge+disk) model, or an exponentially truncated model. We derive some relevant photometric parameters, namely: the asymptotic total magnitude, the effective radius (within which half of the total galaxy luminosity is enclosed), the effective mean surface brightness, the light concentration index C_{31}, and the bulge to total flux ratio for the two-component models. Moreover, using observations taken in optical bands, we compare light profiles in B, V and H, and present color profiles. Combining the present results with those given in Paper V, we obtain a nearly complete sample, covering all morphological types and spanning 4 decades in luminosity.

Table 1. Sample completeness.

	$m_{\rm p}<14$		$m_{\rm p}<15$		$m_{\rm p}<16$		$m_{\rm p}<18$	
	$N_{\rm obs}$	%	$N_{\rm obs}$	%	$N_{\rm obs}$	%	$N_{\rm obs}$	%
Coma S.C.	21	(96)	176	(99)	503	(98)	–	–
Virgo (ISO)	96	(98)	143	(83)	170	(67)	188	(42)
Virgo	195	(94)	260	(72)	295	(55)	315	(34)

The paper is organized as follows: the sample selection criteria are discussed in Sect. 2. The observations and data reduction are described in Sect. 3. The procedures adopted to derive the light profiles and their fitted models are given in Sect. 4. The results of the present work are given in Sect. 5. Some implications of the present analysis on the structural properties of galaxies are discussed in Sect. 6 and summarized in Sect. 7.

2. Sample selection

We report H-band (1.65 μm) observations of 52 faint Virgo galaxies (39 early and 13 late) selected from the VCC catalogue (Binggeli et al. 1985) (restricted to $m_{\rm p} \lesssim 16.0$). With the aim of achieving the highest completeness level, the highest priority was given to objects lying in the region either within 2 degrees of projected radial distance from M 87 or in the corona between 4 and 6 degrees selected by the ISO consortium for complete MIR and FIR observations with ISO (see B97 for a detailed description of this selection criterium). During periods when Virgo was at airmass exceeding 2.2, we observed 20 (17 early and 3 late) galaxies in the Centaurus cluster selected from the CCC as fillers. We also observed two Pec galaxies (CGCG 97-073, 97-087) and the BCD galaxy IZw018.

Adding the present observations to those available from our previous Papers I–IV and B97 of this series, and limiting our sample to the Coma supercluster region ($0.0^{\rm o} \le \delta \le 20.0^{\rm o}$; $11^{\rm h}30^{\rm m} \le \alpha \le 13^{\rm h}30^{\rm m}$) and to the Virgo cluster, the complete subsample with NIR observations is as given in Table 1 in 4 bins of $m_{\rm p}$. The Coma region is completed at the limit of the Zwicky Catalogue. Assuming a distance modulus of Coma of 34.9 ($H_0 = 75\ {\rm km\,s^{-1}\,Mpc^{-1}}$) this corresponds to $M_{\rm p} = -19.2$, i.e. the observations cover a complete sample of giant galaxies. At the distance to the Virgo cluster A of 17 Mpc (Gavazzi et al. 1999), the limiting magnitude $m_{\rm p} = 16$ reached by the present observations corresponds to $M_{\rm p} = -15.2$, i.e. 4 mag deeper than in Coma. However the observations of Virgo can be considered complete down to $M_{\rm p} = -17$, while they are still $\sim$50% complete at $M_{\rm p} = -15$ (slightly better in the ISO subsample). The analysis carried out in Sect. 6 comprises all objects in Table 1.

3. Observations and data reduction

3.1. The observations

The NIR observations reported in this paper were acquired in the photometric nights of March 26th and 27th, 2000 with the 3.6 m, f/11 ESO-NTT telescope, and of December 18th and 19th, 1999 during the science verification period at the 3.6 m, f/11 TNG telescope. The ESO-NTT Nasmyth focus was equipped with the SOFI 1024^2 pixel array camera. With a pixel scale of 0.29 arcsec/pixel, SOFI has a field-of-view of $\sim 5 \times 5$ arcmin. The TNG Nasmyth focus was equipped with the NICMOS3 256^2 pixel array camera ARNICA (Lisi et al. 1993; Lisi et al. 1996; Hunt et al. 1996), which, with a pixel scale of 0.352 arcsec/pixel, gives a field-of-view of $\sim 1.5 \times 1.5$ arcmin.

The seeing at ESO-NTT was always sub-arcsecond, except for one observation taken at a very high airmass (2.14). The mean seeing was 0.77 arcsec ($FWHM$), with a minimum of 0.59 arcsec. At TNG we observed with a mean seeing of 1.5 arcsec.

The NIR sky is extremely bright ($\sim$13 mag arcsec^{-2}) compared with the targets ($\sim$22 mag arcsec^{-2}), with significant fluctuations (up to $10 \div 20\%$ of the mean value) on time-scales comparable with the duration of one observation. In order to observe in linear and background limited regime, observations must be split into several elementary exposures ("coadds") which are averaged together. In order to monitor the sky fluctuations, on-target observations are alternated with off-target observations, following typical pointing sequences ("mosaics").

Depending on the extension of the observed sources, we used two types of mosaic[1]. If the apparent size of the source is similar to the available field of view, half of the observing time was spent on the target, half on the sky. The 8 on-target positions were chosen with slight offsets in order to allow for median rejection of bad pixels. These fields were alternated with 8 sky observations. This was the case of all TNG observations and of some NTT fields in which more than one galaxy could be accomodated into one frame (e.g. 4 Centaurus fields and the galaxy pair VCC1491-1499). Thanks to the large field of view of SOFI compared to the target objects, most of the NTT observations of objects $\lesssim$1.5 arcmin were performed using a second type of mosaic in which the target is always in the field, but is moved around in 6 never overlapping positions, making independent, time costly sky measurements unnecessary. We always avoided to set the object in the north-eastern quadrant of SOFI affected by a lower optical quality.

Table 2 reports the log-book of the observations, including parameters relevant to NIR observations, as follows:
Column (1): VCC (Binggeli et al. 1985), CCC (Jerjen & Dressler 1997) or CGCG (Zwicky et al. 1961-68) denomination.
Column (2): NGC/IC names.
Columns (3), (4): adopted (B1950.0) celestial coordinates, taken from NED[2], with typically one arcsec uncertainty.
Column (5): the morphological type taken from Binggeli et al. (1985), Jerjen & Dressler (1997).
Column (6): the photographic magnitude from the VCC and CCC.
Column (7): the observing date.
Column (8): the telescope used.
Column (9): the number $N_{\rm cds}$ of coadded (averaged) exposures for each frame.
Column (10): the number $N_{\rm cmb}$ of frames combined to obtain the final image.
Column (11): the exposure time for each coadded exposure.
Column (12): the total integration time.
Column (13): the mean airmass during the observation.
Column (14): the adopted filter.
Column (15): the seeing ($FWHM$) in arcsecs.

Optical photometric observations in the B and V passbands for 24 objects in the sample were obtained with the San Pedro Martir (SPM) 2.1 m Telescope from April 20 to 24, 1998 (20 galaxies), and with the Observatoire de Haute Provence (OHP) 120 cm telescope from March 1 to 3, 1998 (4 galaxies, namely VCC608, 745, 1073 and 1254). Both telescopes were equipped with a TK1024 1024^2 pixel CCD camera. The pixel scale is 0.30 arcsec pix^{-1} at SPM, and 0.69 arcsec pix^{-1} at OHP. Exposure times were of 600 s for the V-band and of 900 s for the B-band observations.

3.2. Photometric calibration

Observations of standard stars, from Hunt et al. (1998), and Persson et al. (1998), listed in Table 3, were taken one per hour for calibration purposes.

The calibration stars were observed with a third pointing sequence which consists of five positions, starting with the star near the center of the array, followed by positioning the star in each of the four quadrants of the array. At TNG the telescope was defocussed to avoid saturation, since we observed the two brightest stars of the list. The typical photometric uncertainty is 0.05 mag, both for ESO-NTT and TNG observations.

3.3. Image reduction procedures

The multiplicative system response, or flat-field (FF), was derived for the ESO-NTT observations from a set of dome exposures which allow to remove both the dependence of the dark current level from the illumination of the array and the additive contributions. For the TNG observations, since dome exposures could not be taken, the FF was

[1] Sketches of typical "mosaics" can be found in Fig. 2 of B97.

[2] NASA-IPAC Extragalactic Databasa (NED) is operated by the Jet Propulsion Laboratory, California Institute of Technology, under contract with NASA.

Table 2. The logbook of the observations.

Galaxy	NGC	RA	Dec	Type	m_p	Obs Date	T_{el}	N_{cds}	N_{cmb}	Exp T	Int. T	airm	Filt	seeing
		B1950.0			mag					sec	sec			arcsec
(1)	(2)	(3)	(4)	(5)	(6)	(7)	(8)	(9)	(10)	(11)	(12)	(13)	(14)	(15)
VC0021	I3025	120749.80	+102800.0	dS0	14.75	2000-03-27	NTT	6	12	10	720	1.54	H	0.70
VC0033	I3032	120834.80	+143306.0	dE nuc	14.67	2000-03-28	NTT	10	12	6	720	1.38	H	0.75
VC0048	I3036	120942.10	+124559.0	Sm	14.30	2000-03-28	NTT	10	18	6	1080	1.37	H	0.93
VC0067	I3044	121015.50	+141515.0	dSc pec	13.98	2000-03-28	NTT	10	24	6	1440	1.41	H	0.73
VC0083	I3049	121100.60	+144530.0	Im	15.13	2000-03-27	NTT	6	18	10	1080	1.43	H	0.64
VC0162	I3074	121313.20	+105834.0	Sd	14.41	2000-03-28	NTT	10	24	6	1440	1.71	H	0.74
VC0170	I3077	121323.80	+144240.0	dS0	14.56	2000-03-27	NTT	10	12	6	720	1.73	H	0.71
VC0172	-	121327.60	+045542.0	BCD	14.50	2000-03-28	NTT	6	17	10	1020	1.80	H	0.77
VC0216	I3097	121428.20	+094112.0	dE pec	14.90	2000-03-27	NTT	10	15	6	900	1.86	H	0.90
VC0227	-	121441.40	+091312.0	dE nuc	14.90	2000-03-28	NTT	10	18	6	1080	1.37	H	0.99
VC0275	I3118	121538.40	+094642.0	dS0	14.54	2000-03-28	NTT	10	18	6	1080	2.13	H	0.87
VC0308	I3131	121618.00	+080818.0	dS0 nuc	14.30	2000-03-27	NTT	6	12	10	720	1.31	H	0.71
VC0437	-	121816.20	+174554.0	dE nuc	14.54	2000-03-28	NTT	10	18	6	1080	1.46	H	0.80
VC0620	I3239	122037.20	+120011.0	Sm	15.20	2000-03-27	NTT	10	18	6	1080	1.58	H	0.77
VC0688	N4353	122127.30	+080343.0	dSc	13.94	2000-03-28	NTT	6	12	10	720	1.42	H	0.87
VC0737	-	122206.60	+041636.0	dS/BCD	14.94	2000-03-27	NTT	6	18	10	1080	2.03	H	0.78
VC0750	-	122216.80	+070212.0	dE nuc	14.95	2000-03-27	NTT	6	18	10	1080	1.49	H	0.66
VC0856	I3328	122324.60	+101948.0	dE	14.25	2000-03-27	NTT	6	12	10	720	1.38	H	0.69
VC0951	I3358	122422.20	+115642.0	dE/dS0 pec	14.35	2000-03-27	NTT	10	6	6	360	1.52	H	0.80
VC0975	-	122438.30	+073223.0	Scd	13.58	2000-03-28	NTT	10	24	6	1440	1.67	H	0.90
VC1011	-	122456.50	+075514.0	S0E	14.85	2000-03-27	NTT	10	18	6	1080	1.37	H	0.73
VC1036	N4436	122510.20	+123530.0	dE/dS0 nuc	13.68	2000-03-27	NTT	10	6	6	360	1.42	H	0.73
VC1047	N4440	122521.50	+123411.0	Sa bar	12.48	2000-03-27	NTT	10	2	6	120	1.42	H	0.73
VC1183	I3413	122651.00	+114230.0	dS0 nuc	14.37	2000-03-27	NTT	6	12	10	720	1.44	H	0.67
VC1392	I3459	122922.80	+122660.0	dE/dS0 pec	14.86	2000-03-28	NTT	10	18	6	1080	1.48	H	0.59
VC1491	I3486	123042.40	+130800.0	dE nuc	15.24	2000-03-27	NTT	10	8	6	480	1.41	H	0.81
VC1499	I3492	123048.20	+130744.0	dE pec	14.94	2000-03-27	NTT	10	8	6	480	1.41	H	0.81
VC1514	-	123104.80	+080818.0	dE nuc	15.10	2000-03-27	NTT	6	18	10	1080	1.62	H	0.74
VC1528	I3501	123120.10	+133554.0	dE	14.51	2000-03-28	NTT	10	6	6	360	1.44	H	0.74
VC1549	I3510	123143.20	+112051.0	dE nuc	14.63	2000-03-27	NTT	6	12	10	720	1.31	H	0.64
VC1684	I3578	123407.80	+112242.0	dS0	14.87	2000-03-27	NTT	6	12	10	720	1.34	H	0.78
VC1695	I3586	123422.80	+124800.0	dS0	14.53	2000-03-27	NTT	6	12	10	720	1.34	H	0.61
VC1834	N4600	123749.40	+032338.0	S0 nuc	13.47	2000-03-28	NTT	10	12	6	720	2.09	H	0.87
VC1895	-	123920.40	+094030.0	dE	14.91	2000-03-28	NTT	10	12	6	720	2.10	H	0.87
VC1947	-	124023.30	+035701.0	dE nuc	14.56	2000-03-27	NTT	6	12	10	720	2.04	H	0.93
VC2042	-	124407.20	+093448.0	dE nuc	14.84	2000-03-27	NTT	6	18	10	1080	1.76	H	0.70
VC2050	I3779	124449.80	+122624.0	dE nuc	15.20	2000-03-27	NTT	6	12	10	720	1.34	H	0.67
2MASX[a]	-	120848.10	+143120.0	Im/S	17.24	2000-03-28	NTT	10	4	6	240	1.38	H	0.68
CCC045	-	124537.20	−405103.2	E	14.93	2000-03-27	NTT	10	16	6	960	2.20	H	0.84
CCC059	-	124553.20	−405046.0	dE nuc	18.60	2000-03-27	NTT	10	16	6	960	2.20	H	0.84
CCC094	-	124639.50	−410926.0	dS0 nuc	16.67	2000-03-27	NTT	10	16	6	960	1.61	H	0.84
CCC095	-	124640.20	−411303.0	S0	14.56	2000-03-27	NTT	10	16	6	960	1.61	H	0.84
CCC096	-	124640.70	−411127.4	S0	14.70	2000-03-27	NTT	10	16	6	960	1.61	H	0.84
CCC104	-	124649.80	−410916.0	dE nuc	18.25	2000-03-27	NTT	10	16	6	960	1.61	H	0.84
CCC113	-	124656.00	−405725.0	E	17.33	2000-03-26	NTT	6	16	10	960	2.14	H	1.10
CCC119	-	124705.60	−405714.1	E	14.64	2000-03-26	NTT	6	16	10	960	2.14	H	1.10
CCC122	N4706	124708.10	−410026.3	S0a	14.18	2000-03-26	NTT	6	16	10	960	2.14	H	1.10
CCC125	-	124710.40	−405917.0	dE nuc	17.14	2000-03-26	NTT	6	16	10	960	2.14	H	1.10
CCC136	-	124725.70	−410138.4	E	16.25	2000-03-28	NTT	10	8	6	480	1.71	H	0.84
CCC142	-	124731.30	−410156.0	Sm	18.40	2000-03-28	NTT	10	8	6	480	1.71	H	0.84
CCC150	-	124738.00	−410130.0	dE nuc	18.23	2000-03-28	NTT	10	8	6	480	1.71	H	0.84
CCC153	-	124741.60	−410210.0	dE nuc	18.24	2000-03-28	NTT	10	8	6	480	1.71	H	0.84
CCC157	-	124747.30	−410351.0	Sm	18.23	2000-03-28	NTT	10	8	6	480	1.71	H	0.84
CCC205	-	124901.60	−404321.0	S0	15.95	2000-03-28	NTT	6	6	10	360	1.90	H	0.78
CCC216	-	124915.80	−410454.0	dE nuc	18.22	2000-03-27	NTT	10	16	6	960	1.70	H	0.78
CCC222	-	124926.20	−410402.9	dSc	14.74	2000-03-27	NTT	10	16	6	960	1.70	H	0.78
CCC226	N4743	124929.30	−410708.6	S0a	14.08	2000-03-27	NTT	10	16	6	960	1.70	H	0.78
CEG050[b]	-	124828.10	−410903.0	dE	?	2000-03-27	NTT	10	16	6	960	2.20	H	0.84
VC0010	I3017	120651.70	+135110.0	BCD	14.75	1999-12-19	TNG	6	8	10	480	1.78	H	1.50
VC0608	N4322	122029.70	+161058.0	dE nuc	14.94	1999-12-20	TNG	6	8	10	480	1.90	H	1.30
VC0745	N4366	122214.40	+073748.0	dE nuc	14.67	1999-12-20	TNG	4	5	10	200	1.22	H	1.09
VC0786	I3305	122243.80	+120754.0	dE nuc	15.11	1999-12-20	TNG	6	9	10	540	1.25	H	1.21
VC0965	I3363	122431.20	+125006.0	dE nuc	15.40	1999-12-20	TNG	6	8	10	480	1.77	H	1.27
VC1073	I794	122536.50	+122211.0	dE nuc	14.23	1999-12-20	TNG	6	8	10	480	1.08	H	0.90
VC1078	-	122539.00	+100224.0	dE ?	15.30	1999-12-19	TNG	6	12	10	720	1.20	H	1.06
VC1122	I3393	122609.60	+131130.0	dE nuc	14.60	1999-12-19	TNG	4	8	10	320	1.76	H	1.90
VC1173	-	122643.00	+131516.0	dE nuc	16.06	1999-12-20	TNG	6	8	10	480	1.58	H	1.76
VC1254	-	122732.80	+082103.0	dE nuc	15.51	1999-12-20	TNG	6	8	10	480	1.15	H	0.88
VC1308	I3437	122814.40	+113700.0	dE nuc	15.64	1999-12-20	TNG	4	8	10	320	1.46	H	1.17
VC1348	I3443	122843.90	+123628.0	dE pec	15.87	1999-12-20	TNG	4	8	10	320	1.36	H	1.12
VC1386	I3457	122919.20	+125600.0	dE nuc	14.32	1999-12-19	TNG	4	10	10	400	1.51	H	1.13
VC1453	I3478	123012.80	+142819.0	dE nuc	14.34	1999-12-19	TNG	4	8	10	320	1.63	H	1.48
VC1491	I3486	123042.40	+130800.0	dE nuc	15.24	1999-12-19	TNG	6	8	10	480	1.36	H	1.10
97073	-	114020.75	+201438.1	pec	15.60	1999-12-19	TNG	6	8	10	480	1.67	H	1.27
97087	-	114113.19	+201449.1	pec	14.30	1999-12-20	TNG	3	11	10	330	1.62	H	1.31
1ZW018	-	093030.10	+552747.0	BCD	16.08	1999-12-20	TNG	6	8	10	480	1.28	H	1.10

[a] 2MASX1J1211211+141438,
[b] [BCS89] 050.

obtained averaging, and normalizing to their median counts, a large number ($\gtrsim$30) of sky frames taken throughout the night, with mean levels differing by less than 5%.

The image reduction procedure was as follows. For each target frame the sky contribution was determined and subtracted. This was done by combining, with a

Table 3. Standard calibration stars.

Star	$H_{\rm mag}$
AS 08_0	8.723 ± 0.014
AS 18_0	12.402 ± 0.004
AS 21_0	9.043 ± 0.015
AS 27_1	12.677 ± 0.024
AS 29_1	13.566 ± 0.019
AS 31_1	12.131 ± 0.011
P550_C	12.121 ± 0.005

median sigma clipping algorithm, as many as possible contiguous sky exposures, unless their count level differed by more than 10% from the target frame. In the case of mosaics with the source always in the field, all frames were treated as sky frames. The median sigma clipping algorithm is necessary to remove unwanted star and galaxy images in the resulting sky frames. The sky frame was first normalized to its median, then multiplied by the median counts of the individual target frames. Finally, the rescaled frame was subtracted from the target observation. Such a procedure accounts for temporal variations in the sky level, but introduces an additive offset which is subsequently removed (see below). The sky-subtracted target frames were then divided by the FF frame. Each of the corrected frames was analyzed for low-spatial-frequency gradients, and if necessary, fitted with a two-dimensional 3 degree polynomial which was then subtracted. If this process was not effective in removing the spatial gradients, the corresponding frames were rejected from further analysis. The corrected frames were then aligned using field stars and combined with a median filter with sigma clipping, which allows bad pixel removal.

Finally the residual sky background in the combined frame was determined as the mean number of counts measured in regions of "empty" sky, and it was subtracted from the frame.

All image reduction and analysis was performed in the IRAF environment and relied on the STSDAS package[3], and on GALPHOT (developed for IRAF–STSDAS mainly by W. Freudling, J. Salzer, and M. P. Haynes and adapted by us to handle NIR data).

The final images, with superposed isophotes, are shown in Figs. 1–2.

4. Profile decomposition procedures

The 2-dimensional light distribution of each galaxy was fitted with elliptical isophotes, using a procedure based on the task *ellipse*, (STSDAS *ISOPHOTE* package; Jedrzejewski 1987; Busko 1996), which allows the interactive masking of unwanted superposed sources. Starting from an interactively centered ellipse, the fit maintains as free parameters the ellipse center, ellipticity, and position angle. The ellipse semi-major axis is incremented by a fixed fraction of its value at each step of the fitting procedure. The routine halts when the surface brightness found in a given corona equals the sky rms, and then restarts decrementing the initial semi-major axis toward the center. Isophotes whose rms is greater than their mean value are discarded. The fit fails to converge for some galaxies with very irregular light distributions. In these cases we kept fixed one or more of the ellipse parameters.

The resulting radial light profiles were fitted using one of four models of light distributions:
1) a de Vaucouleurs $r^{1/4}$ law (de Vaucouleurs 1948);
2) an exponential law;
3) a "mixed" profile consisting of the sum (in flux) of an exponential law, dominating at large radii ("disk"), and an exponential or a de Vaucouleurs $r^{1/4}$ law, dominating at small radii ("bulge");
4) a "truncated" profile consisting of an exponential or a de Vaucouleurs $r^{1/4}$ law, truncated by a steeper exponential law beyond a certain critical radius $r_{\rm t}$, according to either of the following:

$$I(r) = c_1 \cdot \exp\big[-\frac{1}{c_2}(r - r_{\rm t} - |r - r_{\rm t}|)\big] \times \exp\big[-\frac{1}{c_3}(r - r_{\rm t} + |r - r_{\rm t}|\big] \text{ (Truncated exponential)}$$

$$I(r) = c_1 \cdot \exp\big[-\frac{1}{c_2}(r^{1/4} - r_{\rm t}^{1/4} - |r^{1/4} - r_{\rm t}^{1/4}|)\big] \times \exp\big[-\frac{1}{c_3}(r - r_{\rm t} + |r - r_{\rm t}|\big] \text{ (Tr. DeVaucouleurs).}$$

For pure de Vaucouleurs and exponential laws, the fit was performed using a weighted least squares method. For the mixed and truncated profiles, the fit was performed using the Levemberg-Marquardt algorithm implemented in the task *nfit1d* (STSDAS *FITTING* package). This algorithm is implemented within an interactive procedure which requires some initial set of parameters i.e. 4 markers delimiting the outer or exponential dominated region, and the inner or bulge dominated region. The former is fitted with an exponential law. For mixed profiles, the external exponential fit is extrapolated to the inner region and subtracted. The resulting inner profile is then fitted either with an exponential or a de Vaucouleurs $r^{1/4}$ law, according to a χ^2 test. Fitting parameters are then assumed as initial guess for the Levemberg-Marquardt algorithm. For truncated profiles, the inner region is fitted either with an exponential or a de Vaucouleurs $r^{1/4}$ law, according to a χ^2 test, and the fitting parameters are then used as initial guess, along with the external exponential slope and the inner edge of the outer region as $r_{\rm t}$.

The fits are performed from a radius equal to twice the seeing disk, out to the outermost significant isophotes.

[3] IRAF is the Image Analysis and Reduction Facility made available to the astronomical community by the National Optical Astronomy Observatories, which are operated by AURA, Inc., under contract with the U.S. National Science Foundation. STSDAS is distributed by the Space Telescope Science Institute, which is operated by the Association of Universities for Research in Astronomy (AURA), Inc., under NASA contract NAS 5–26555.

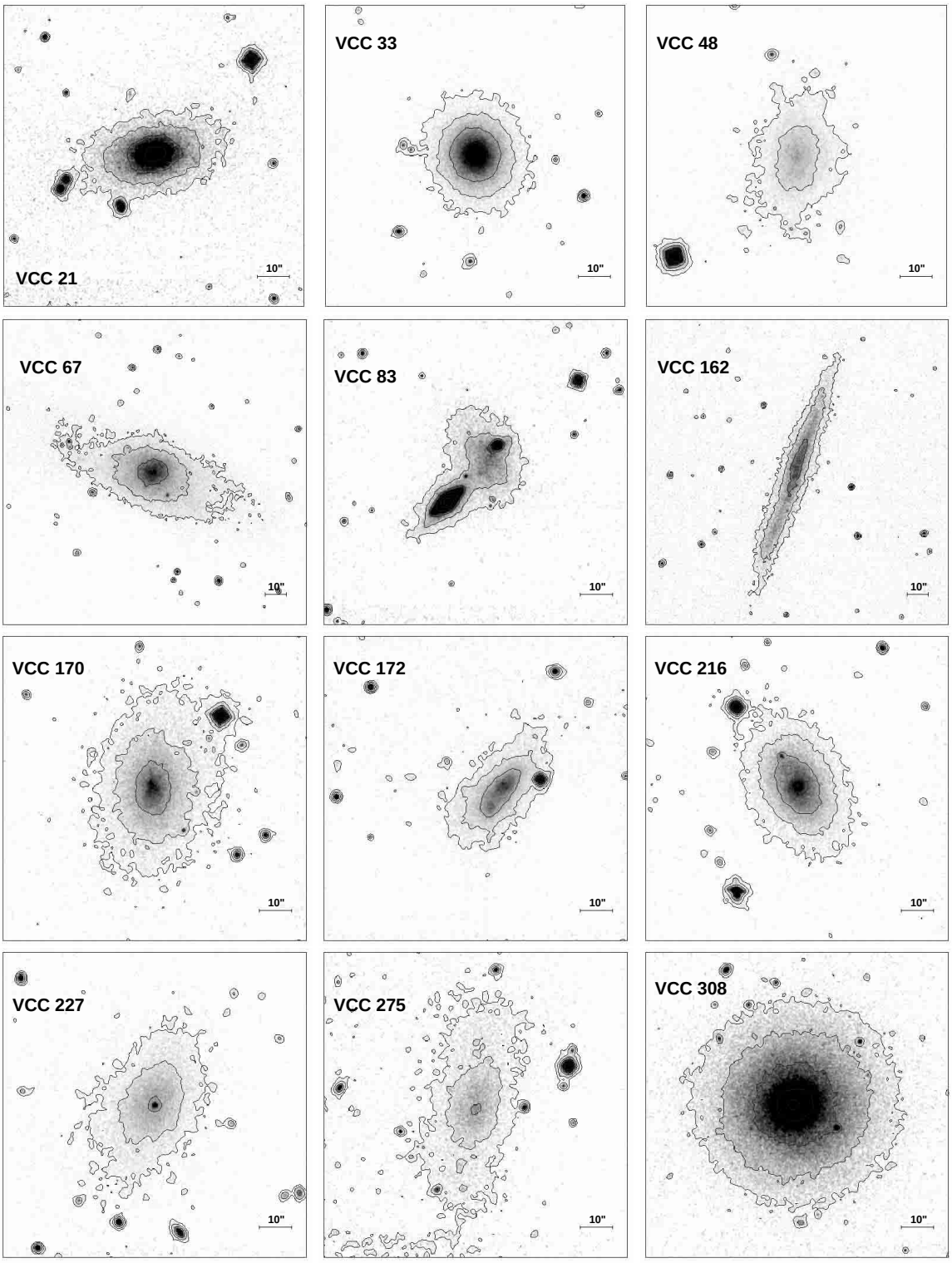

Fig. 1. ESO-NTT images. North is up, East to the left. Contours are drawn from 21.5 mag arcsec^{-2}, in steps of 1 mag arcsec^{-2}.

Total magnitudes $H_{\rm T}$ are then obtained by adding to the flux measured within the outermost significant isophote the flux extrapolated to infinity along the fitted profile. The $1-\sigma$ error attached to the total magnitude $H_{\rm T}$ combines the statistical error on the flux at the outermost isophote with that on the fit parameters.

The effective radius $r_{\rm e}$ (the radius containing half of the total light) and the effective surface brightness $\mu_{\rm e}$ (the mean surface brightness within $r_{\rm e}$) of each galaxy are "empirically" computed (see Paper V). The relative errors are obtained combining the uncertainty on $H_{\rm T}$, as described above, with the scatter $\sigma_{\rm r}$ along the integrated-light growth curve.

Finally we compute other useful parameters: the concentration index (C_{31}), defined in de Vaucouleurs (1977) as the model–independent ratio between the radii that

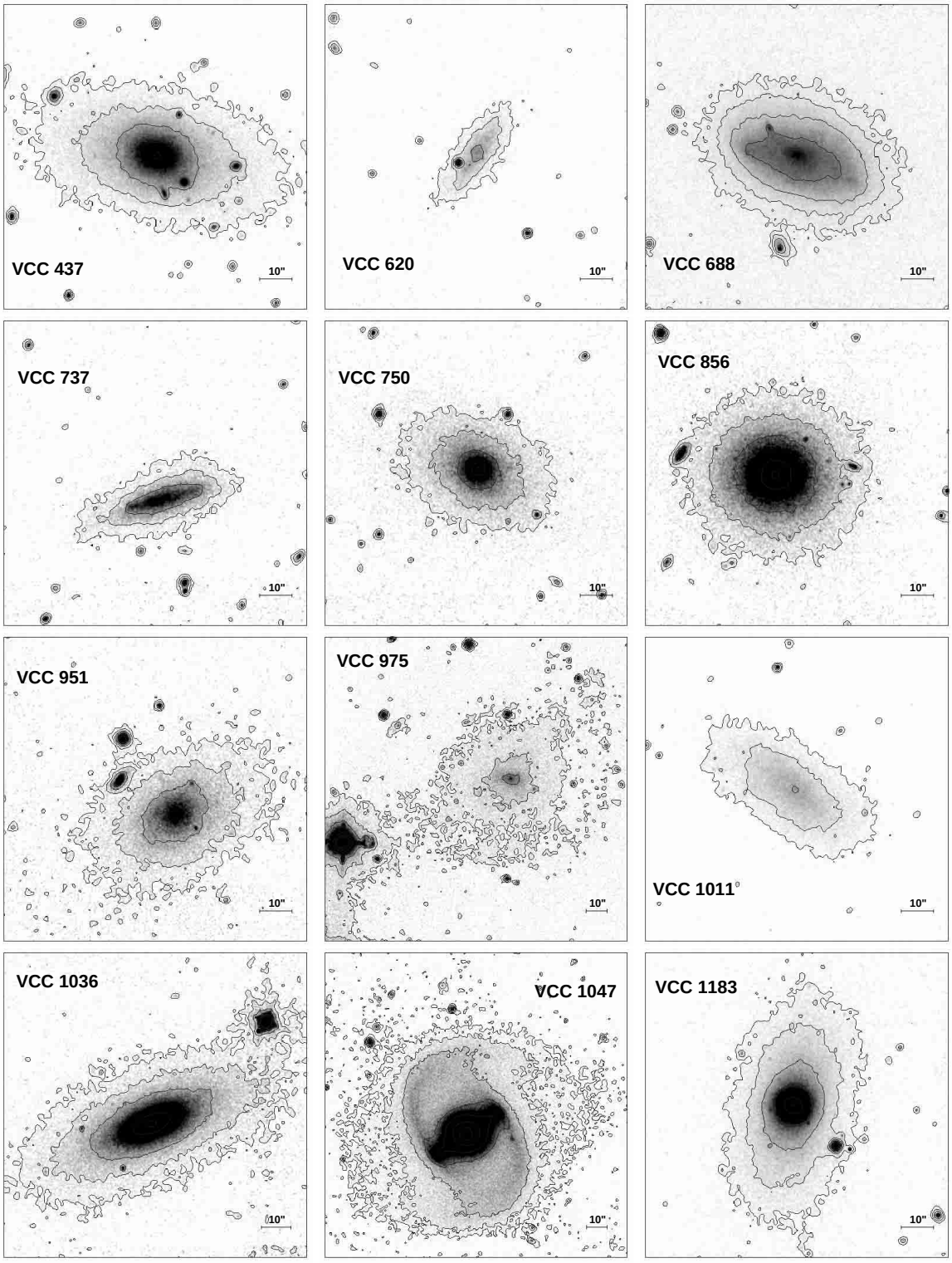

Fig. 1. continued.

enclose 75% and 25% of the total light $H_{\rm T}$, and, for galaxies fitted with a two component model, the bulge to total flux ratio (B/T).

The derived surface brightness profiles are shown in Fig. 3: each galaxy is labelled with a prefix denoting the telescope (N00 for ESO-NTT or G99 for TNG), followed by its catalogue name and by the type of decomposition (see Table 4).

5. Results

The results of the present work are summarized in Table 4, as follows:
Column 1: VCC (Binggeli et al. 1985) or CCC (Jerjen & Dressler 1997) or CGCG (Zwicky et al. 1961-68) designation.
Column 2: adopted filter (B or H).

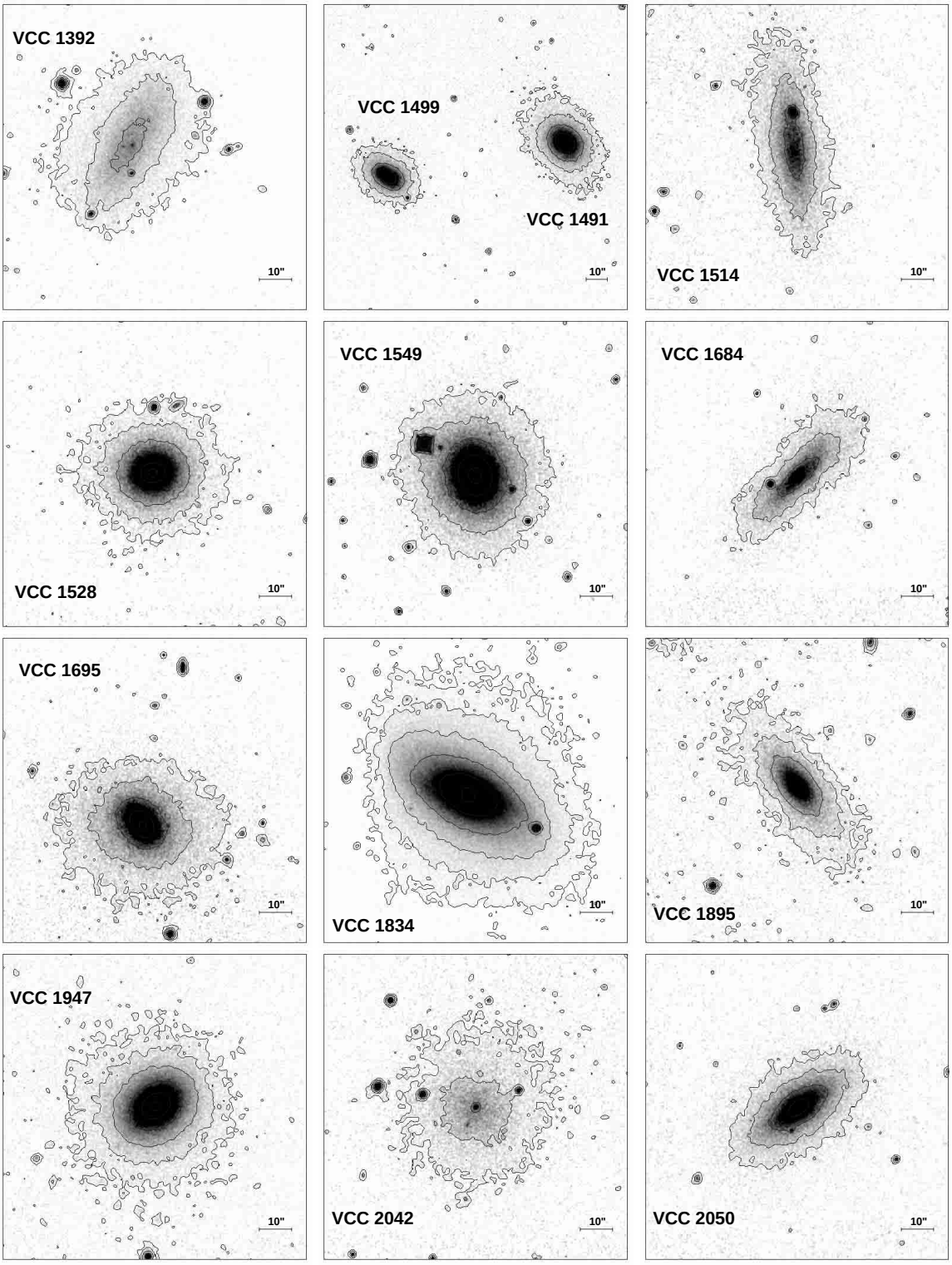

Fig. 1. continued.

Column 3: type of decomposition: D = pure de Vaucouleurs; E = pure exponential; M = mixed; T = truncated.
Column 4: nucleus: Y = present, not fitted; N = absent; B = extended, fitted as a bulge.
Column 5: type of decomposition of the bulge: D = de Vaucouleurs; E = exponential.
Column 6: effective radius of the fitted bulge component ($r_{\rm ebf}$) in arcsec.
Column 7: effective surface brightness of the fitted bulge component ($\mu_{\rm ebf}$) in mag arcsec^{-2}.
Column 8: effective radius of the fitted disk component ($r_{\rm edf}$) in arcsec.
Column 9: effective surface brightness of the fitted disk

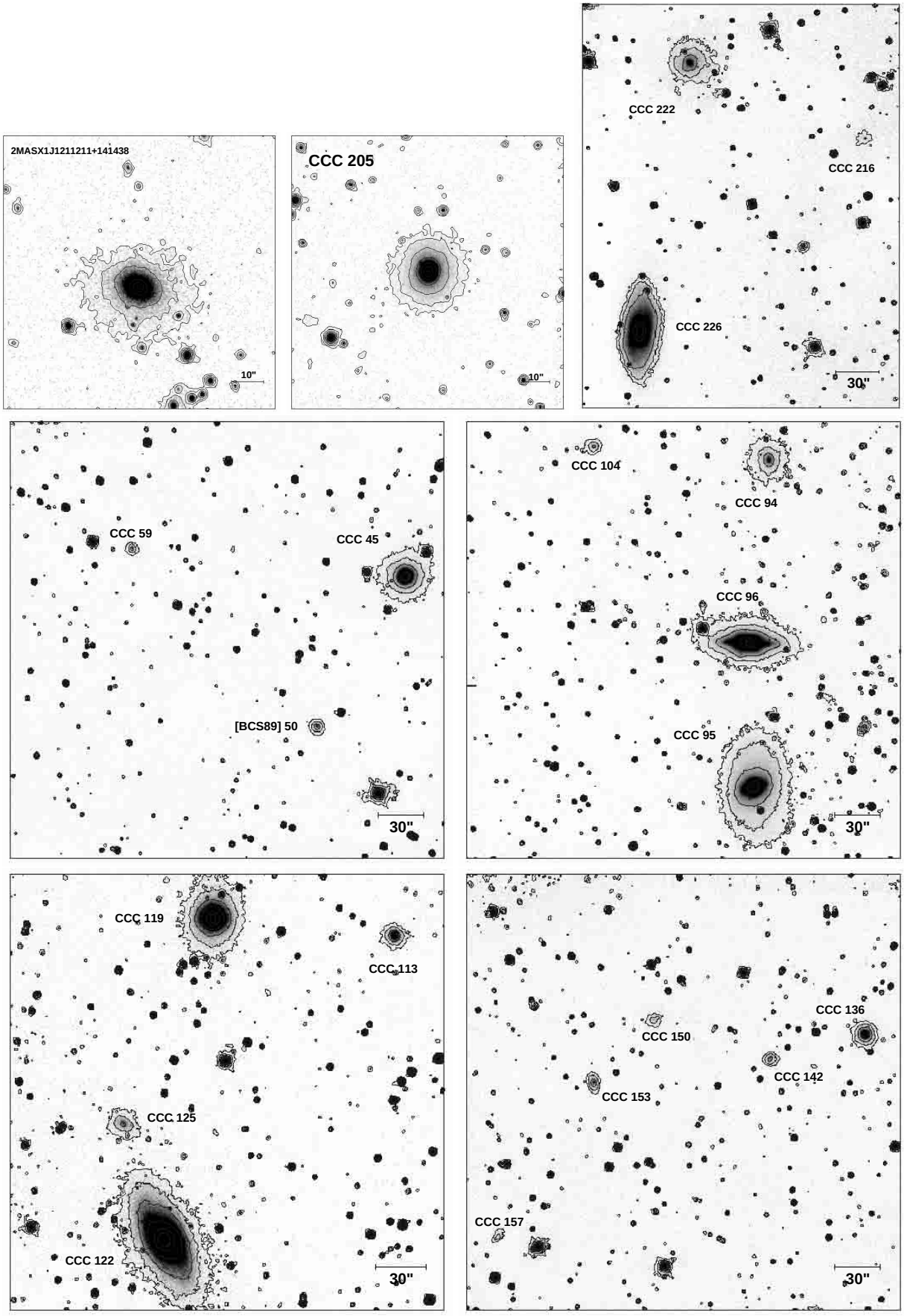

Fig. 1. continued.

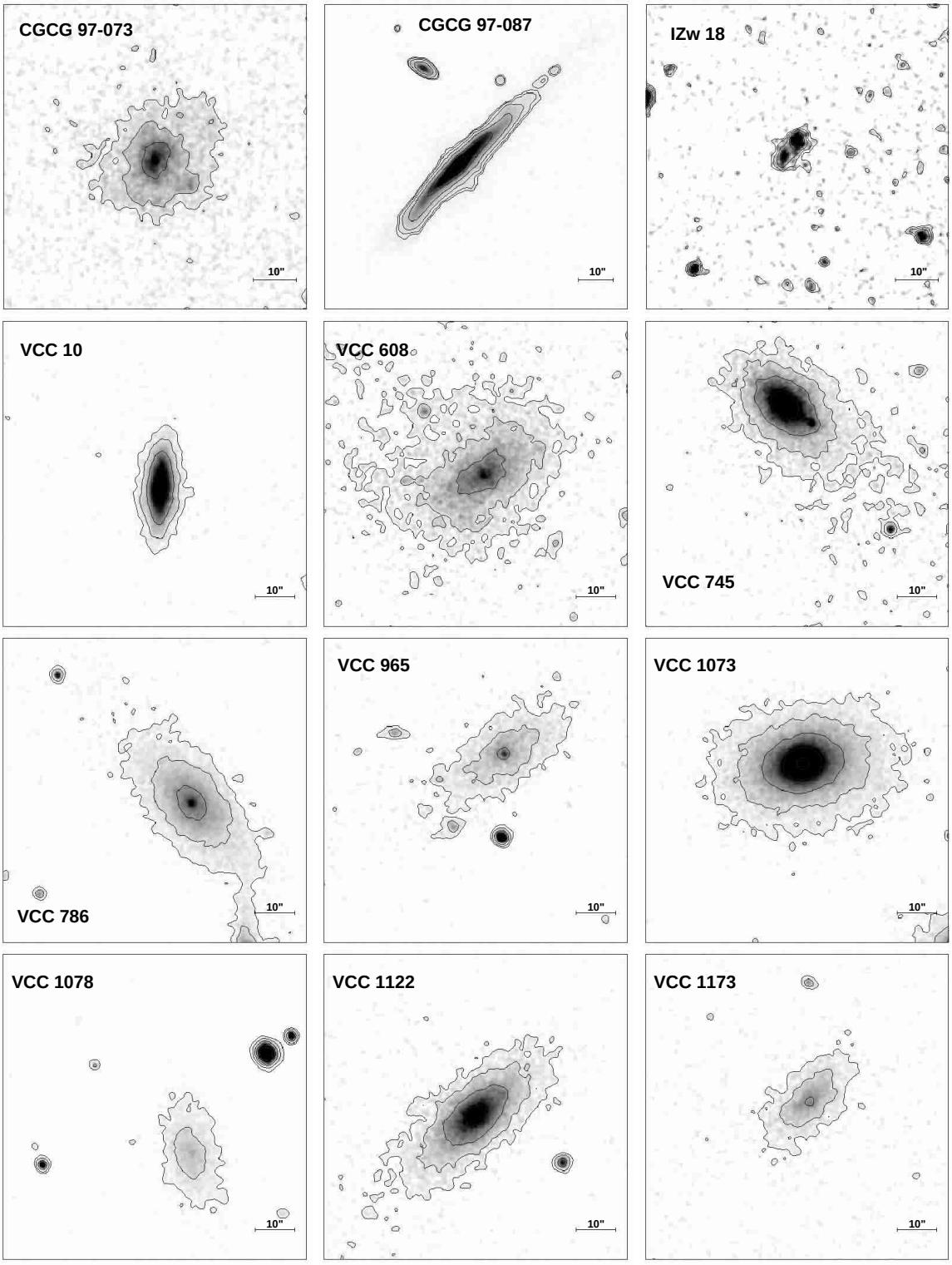

Fig. 2. TNG images. North is up, East to the left. Contours are drawn from 21.0 mag arcsec^{-2}, in steps of 1 mag arcsec^{-2} (except for IZw018 whose fainter isophote is 21.5 mag arcsec^{-2}).

component ($\mu_{\rm edf}$) in mag arcsec^{-2}.
Column 10: effective radius of the fitted outer exponential component ($r_{\rm eout}$) in arcsec given for truncated profiles.
Column 11: effective surface brightness of the fitted outer exponential component ($\mu_{\rm eout}$) in mag arcsec^{-2}.
Columns 12–13: total effective radius ($r_{\rm e}$) and associated uncertainty in arcsec.
Columns 14–15: total effective surface brightness ($\mu_{\rm e}$) and associated uncertainty in mag arcsec^{-2}.
Columns 16–17: total magnitude ($m_{\rm T}$) extrapolated to infinity and associated uncertainty.
Columns 18–19: concentration index (C_{31}) and associated

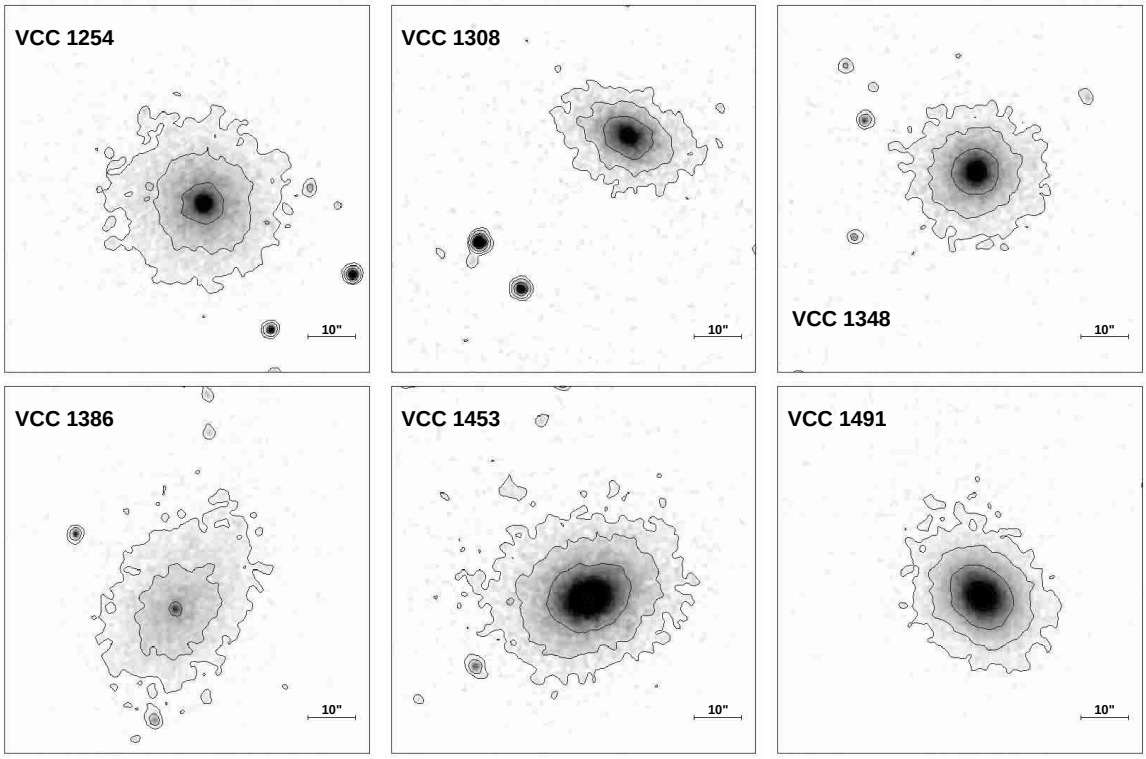

Fig. 2. continued.

uncertainty.
Column 20: bulge to total flux ratio (B/T).

6. Analysis

The analysis presented in this Sect. is based on 818 galaxies listed in Table 1. Assuming an average $B-H=3$ mag, the optical completeness levels given in Sect. 2 translate into 100% completeness at Log $L_{\rm H_\odot} > 10$ for the Coma supercluster, 100% at Log $L_{\rm H_\odot} > 9.4$ and 50% at Log $L_{\rm H_\odot} > 8.6$ for the Virgo cluster. The 50% unobserved Virgo galaxies with $16.0 > m_{\rm p} > 14.0$ mag includes objects whose surface brightness, as judged on the DSS plates, was fainter than what we could expect to detect with a 4 m telescope in one-hour integration.

6.1. The frequency of profile decompositions

We consider the distribution of profile decompositions along the Hubble sequence only for galaxies in the Virgo cluster, for which the morphological classification is most reliable. This is shown in Fig. 5. It is apparent that pure de Vaucouleurs profiles are present only in 40% of Es and in 30% of S0s. Their contribution drops to zero both for later types and for the early type dwarfs. The exponential profiles are nearly absent among early type giant systems up to Sab, while their frequency is high (44%) in dwarf E+S0s, and increases from 40% (Sc) to almost 100% for later types. Mixed (M) decompositions dominate among dwarf E and S0s (50%) and giant Es (50%), increasing up to 90% among Sb galaxies, then drop to zero for later types. Truncated profiles (T) are rare (their frequency is always <35%), and are absent from giant early-type galaxies up to Sc spirals.

Figure 6 shows the relative fraction of profile decompositions plotted as a function of the H band luminosity (Log $L_{\rm H}/L_\odot = 11.36 - 0.4H_{\rm T} + 2{\rm Log}\,D$ (D in Mpc)) for the 818 objects in the Virgo+Coma sample (top-left panel), for the early type (dE-E-S0a) (bottom-left panel), late type (Sa-BCD) (bottom-right panel) and Sc-Sd galaxies alone (top-right panel). All panels show similar trends, indicating that the dependence of the frequency of profile decompositions on luminosity is independent of the morphological type. The fraction of pure de Vaucouleurs profiles strongly increases with the H luminosity, being absent for $L_{\rm H} < 10^{9.5}\ L_\odot$, a luminosity range where the pure exponential profiles dominate, since their frequency clearly anti-correlates with luminosity. At the faintest luminosities, however truncated profiles are abundant among late-type galaxies. The frequency of mixed profiles increases monotonically with luminosity among late-type galaxies, while it reaches a maximum at $L_{\rm H} \sim 10^{10}\ L_\odot$ for the early-type ones, because for higher luminosities these galaxies have increasingly more frequently pure de Vaucuoleurs profiles.

6.2. The light concentration parameter C_{31}

Figure 7 shows the remarkable dependence of C_{31} on luminosity found by Scodeggio et al. (in preparation) and extended here to comprise dwarf galaxies. We confirm that high C_{31} (cusps+extended haloes) are almost completely

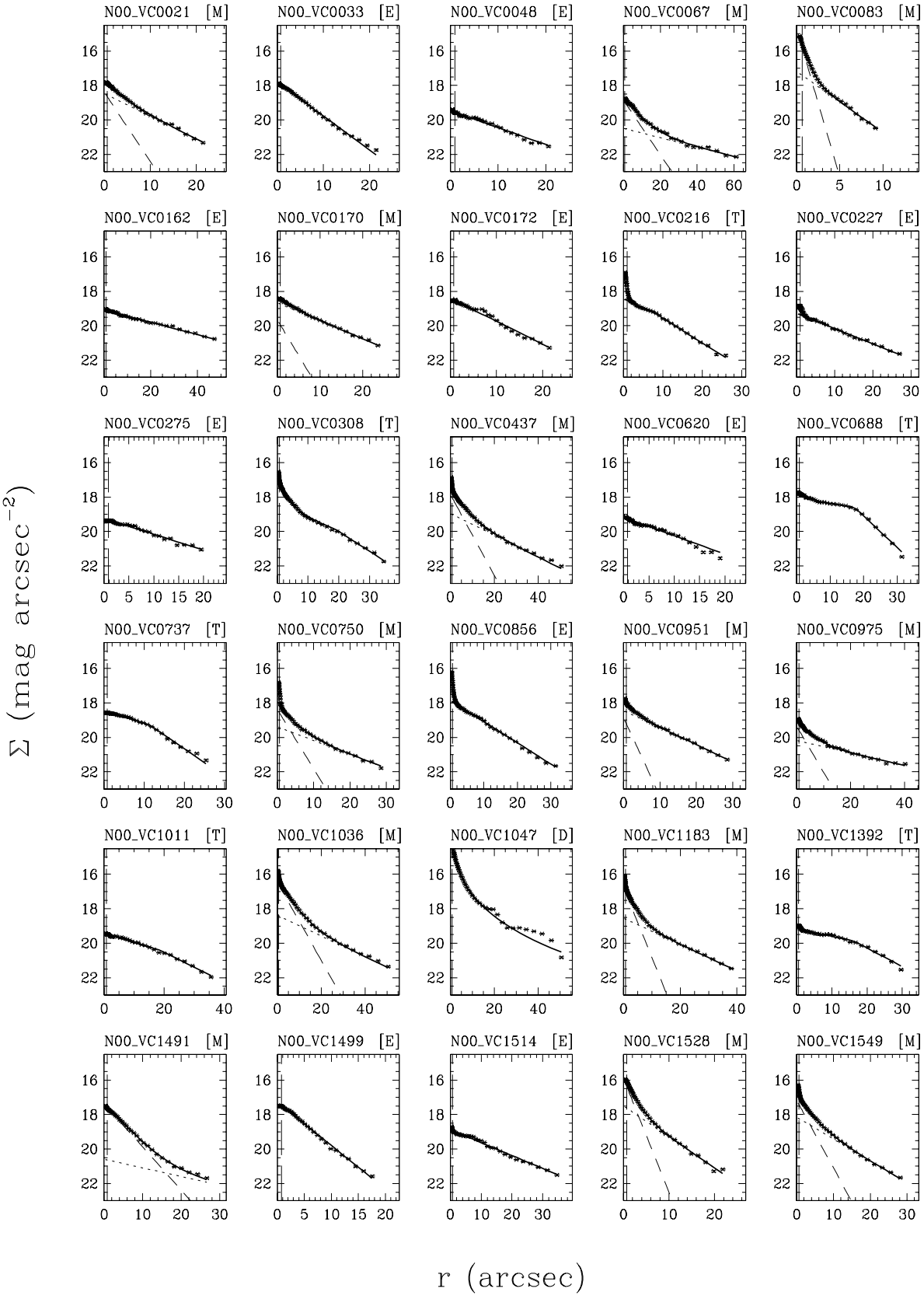

Fig. 3. The surface brightness profiles (dots). The solid line is the fitted profile; the dashed and the dotted lines represent the bulge and disk component respectively. The vertical dashed line represents the seeing disk.

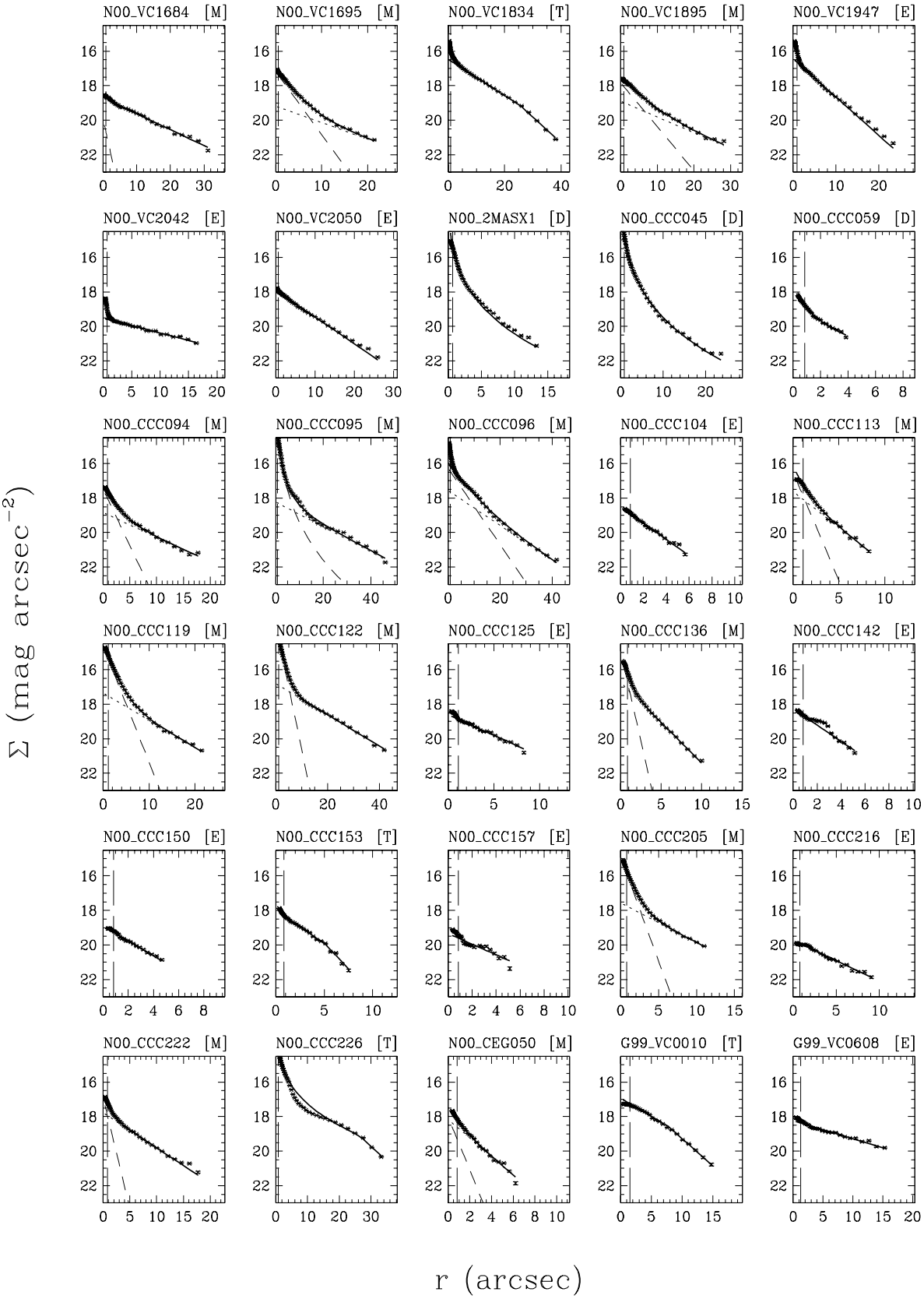

Fig. 3. continued.

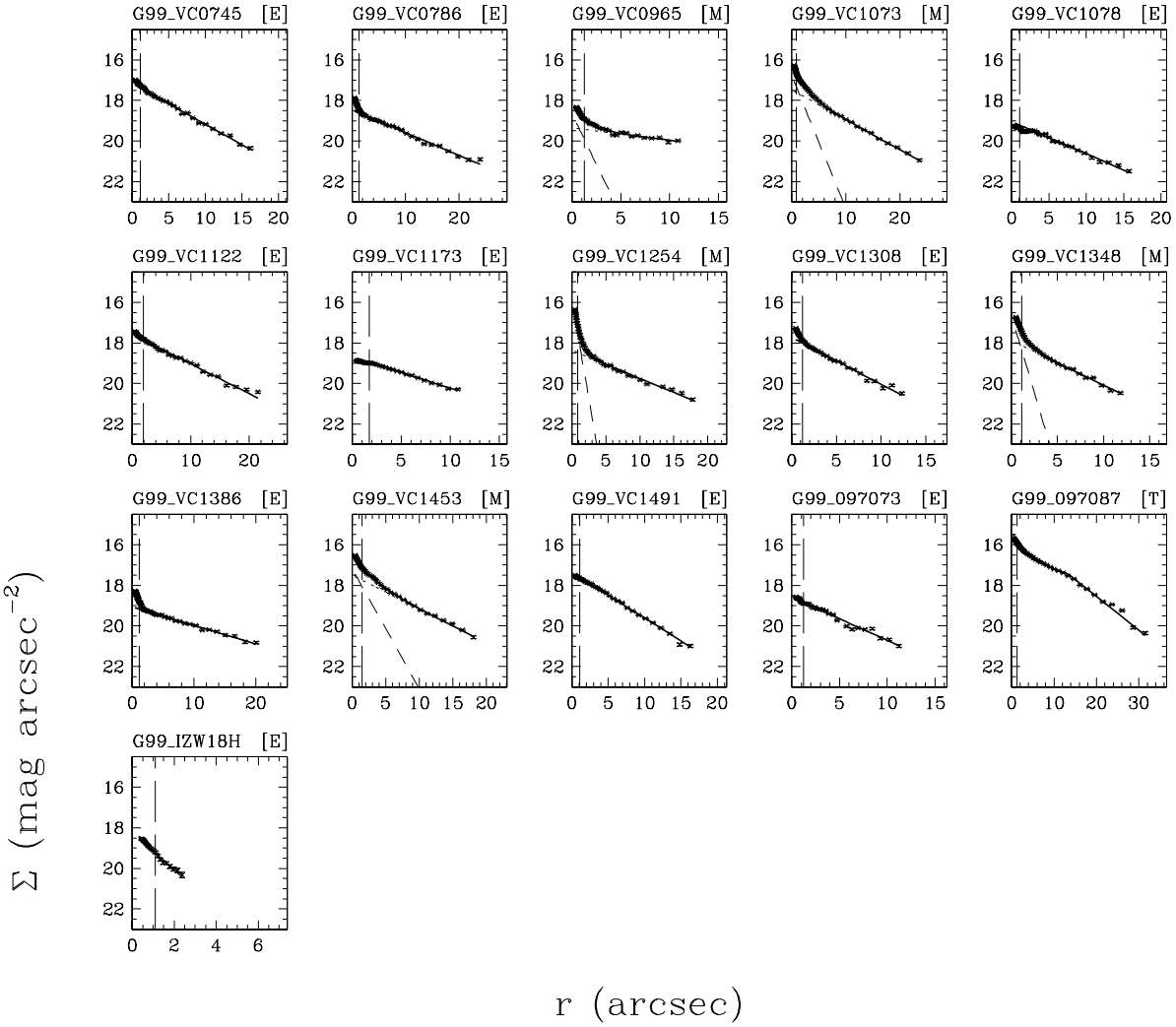

Fig. 3. continued.

absent at $L_{\rm H} < 10^{9.5}\ L_\odot$. Faint galaxies cluster around $C_{31} = 2.80$, which is the expected value for pure exponential profiles. This result is completely independent from galaxy morphology. On the other end high C_{31} (bulge-dominated) objects are present only at high luminosity $L_{\rm H} > 10^{10.5}\ L_\odot$. These are a mixture of giant E and Early-type spirals. There exist however a significant class of high-luminosity (giant), low C_{31} (bulge-less) galaxies which appears to be confined to Sc galaxies.

6.3. Color gradients

Only 22 dE/dS0 in Virgo analyzed in this paper have either $B-V$ or $B-H$ color profile (see Fig. 4). Nine among these 22 (41%) have no radial color gradients. Another 9 have a red central excess consistent with an age or metallicity gradient toward the center. The remaining 4 (VCC 781, 951, 1499, 1684, representing a non-negligeable 18% of our sample) have instead a blue central excess consistent with a nuclear post star-burst phase (see below the discussion on VCC 1499). In spite of the paucity of the available data, we find that the color of the central excess correlates with the global color ($< B-V >_{\rm Bexcess} = 0.61$, $< B-V >_{\rm Rexcess} = 0.82$) and that the 4 $B_{\rm excess}$ objects have on average slightly lower $< L_{\rm H} > = 8.9$ than those with $R_{\rm excess}$ ($< L_{\rm H} > = 9.1$).
This evidence is consistent with the analysis by Kormendy & Djorgovski (1989) (see their Fig. 4).

We also find that the color distribution of dEs overlaps with that of dIs (see Fig. 8), though the mean colors of the two groups differ significantly.

Excluding galaxies with $m_{\rm p} > 16.0$, because we don't have measurements of dEs fainter than this limit, we explored the possible continuity in the structural parameters of dEs and dIs, as proposed by Sung et al. (1998). dEs (9 objects) and nucleated dE-Ns (27 objects) are indistinguishable from each other both in colors ($< B-H > \ \sim 3.1$) and in C_{31} ($< C_{31} > \sim 3.4$). The only subclass of dEs with significantly bluer colors and lower C_{31} are dE-pecs (6 objects) which have $< B-H > \sim 2.7$ and $< C_{31} > \sim 2.7$, consistent with $< B-H > \sim 2.5$ and $< C_{31} > \sim 2.5$ of dIs (16 objects).

An illustrative and meaningful example of the wide range spanned in color and color gradient by dEs is offered

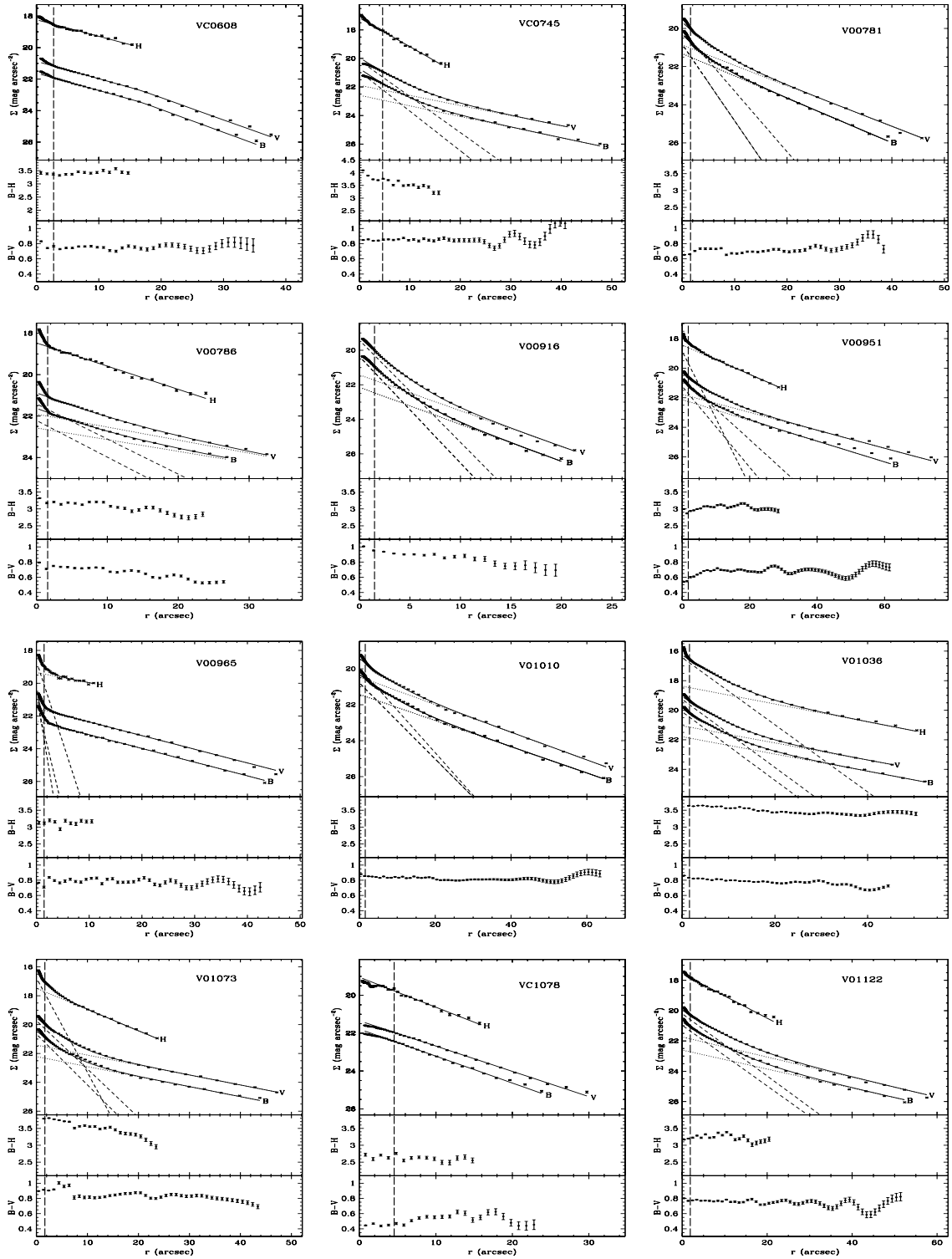

Fig. 4. Radial light and color profiles of 24 galaxies having at least 2 band measurements. The vertical dashed line represents the seeing disk of the optical observations.

by the two galaxies VCC1491 and 1499 which happen to lie 1.5 arcmin apart in the same frame (see Fig. 1). The two have V mag differing by 0.01 mag, thus they are indistinguishable galaxies in all respects. However VCC1491 is almost as red ($B-V=0.82$, $B-H=3.42$) as a giant elliptical, while on the opposite VCC1499 (dE-pec) is almost as blue ($B-V=0.49$, $B-H=2.67$) as a typical dI. Moreover VCC1499 shows a strong blue central excess, while VCC1491 presents a shallower red gradient toward its centre (see Fig. 9 and profiles in Fig. 4). Using the Carelec spectrograph (Lemaitre et al. 1990) attached to the OHP 1.93 m telescope we obtained in February 2000

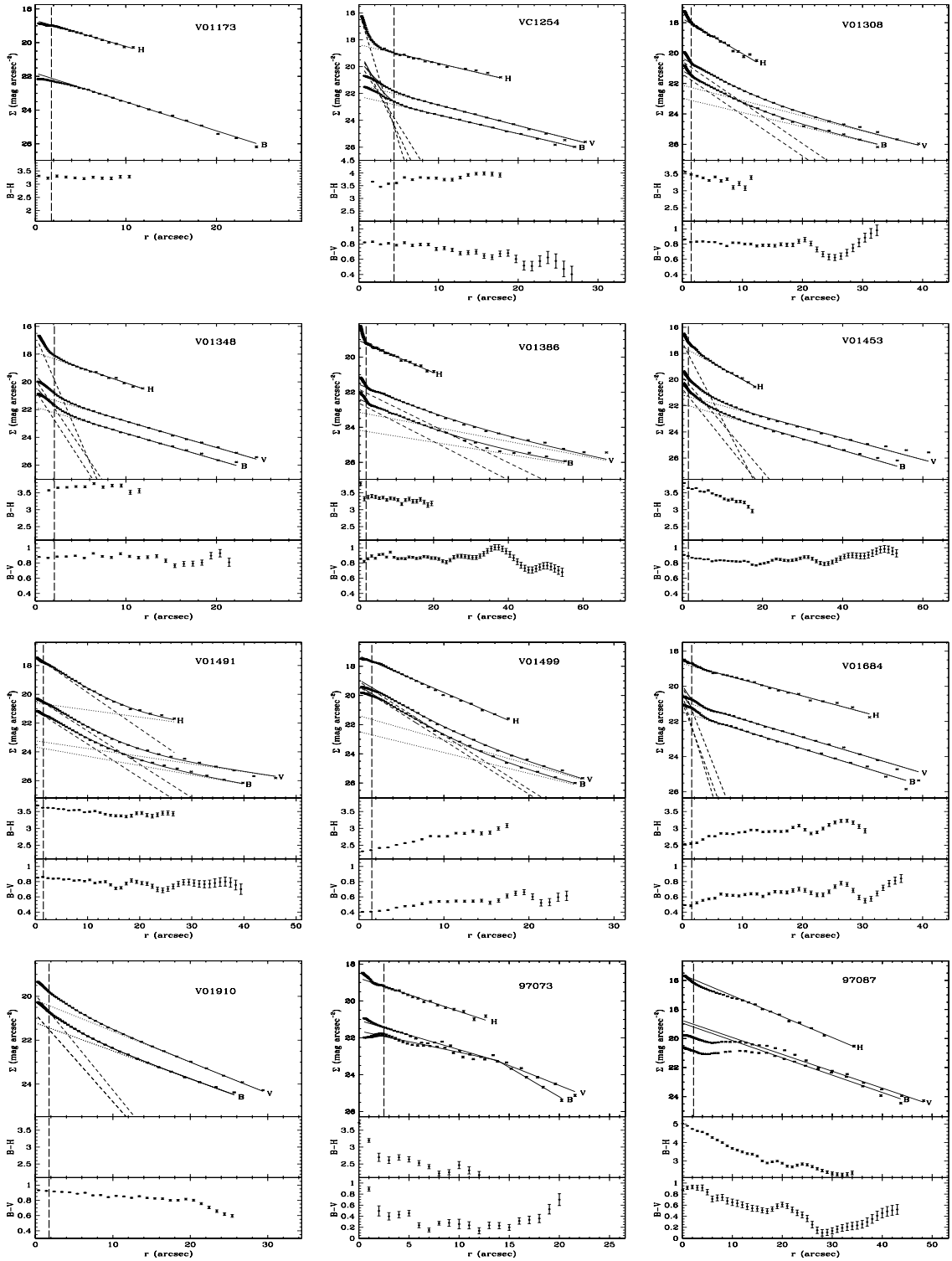

Fig. 4. continued.

long slit spectra for the two objects, shown in Fig. 10. The spectral signatures of the two galaxies are significantly different: 1491 resembles a typical dE galaxy, while 1499 has a much bluer continuum and strong Balmer absorption lines (EW $H_\delta \sim 8$ Å) typical of E+A galaxies which have experienced an intense burst of star formation ended about 1–2 Gyrs ago (Poggianti & Barbaro 1996).

7. Summary and conclusions

We obtained near-infrared H-band profile decompositions for 75 galaxies taken primarily among dwarf galaxies in the Virgo cluster. Adding these new observations to the ones similarly taken in the Virgo, Coma and A1367 clusters and in the "Great Wall" (Paper V), we gathered

Table 4. Photometric parameters of the target galaxies.

					Bulge		Disk exp		Outer exp											
Galaxy	Filter	dec	Nuc	Bdec	r_{ebf} arcsec	μ_{ebf} mag/□"	r_{edf} arcsec	μ_{edf} mag/□"	r_{eout} arcsec	μ_{eout} mag/□"	r_e arcsec	±	μ_e mag/□"	±	M_T mag	±	C_{31}	±	B/T
(1)	(2)	(3)	(4)	(5)	(6)	(7)	(8)	(9)	(10)	(11)	(12)	(13)	(14)	(15)	(16)	(17)	(18)	(19)	(20)
VC0010	H	T	N	E	-	-	8.63	18.05	5.74	17.23	7.0	1.0	17.86	0.28	12.76	0.07	2.65	0.03	0.59
VC0021	H	M	N	E	4.50	19.49	13.67	19.57	-	-	12.0	1.2	19.16	0.18	12.33	0.07	3.31	0.01	0.09
VC0033	H	E	N	-	-	-	9.17	18.90	-	-	8.7	1.1	18.77	0.23	12.24	0.07	2.79	0.02	0.00
VC0048	H	E	N	-	-	-	18.55	20.58	-	-	19.2	1.1	20.65	0.10	12.72	0.06	2.70	0.03	0.00
VC0067	H	M	N	E	11.48	19.97	66.67	21.60	-	-	53.8	6.0	20.98	0.19	11.27	0.08	5.55	0.14	0.18
VC0083	H	E	N	E	-	-	15.47	20.56	-	-	15.4	1.1	20.55	0.13	12.98	0.06	2.84	0.01	0.00
VC0162	H	E	N	-	-	-	50.45	20.19	-	-	62.2	2.0	20.91	0.06	11.48	0.06	2.44	0.02	0.00
VC0170	H	M	N	E	4.37	20.75	17.41	19.77	-	-	17.0	1.1	19.71	0.11	11.98	0.06	2.80	0.02	0.02
VC0172	H	E	N	-	-	-	13.73	19.53	-	-	13.5	1.1	19.60	0.15	12.68	0.06	2.80	0.01	0.00
VC0216	H	T	Y	E	-	-	16.86	19.53	12.65	19.24	12.8	1.2	19.30	0.17	12.21	0.06	2.76	0.00	0.28
VC0227	H	E	Y	-	-	-	20.33	20.38	-	-	21.0	1.3	20.51	0.11	12.33	0.06	3.17	0.02	0.00
VC0275	H	E	N	-	-	-	19.80	20.35	-	-	18.9	1.1	20.19	0.10	12.54	0.06	3.10	0.01	0.00
VC0308	H	T	B	D	143.68	21.77	-	-	15.77	18.81	17.1	1.2	19.10	0.12	11.00	0.06	3.01	0.01	0.54
VC0437	H	M	Y	E	7.69	18.94	28.63	20.06	-	-	20.0	1.5	19.12	0.13	11.22	0.06	4.38	0.11	0.21
VC0608	B	T	Y	E	-	-	16.47	22.73	12.49	22.13	15.7	1.2	22.83	0.12	15.29	0.07	2.67	0.02	0.59
VC0608	H	E	Y	-	-	-	17.26	19.34	-	-	17.7	1.1	19.43	0.11	11.87	0.06	2.66	0.01	0.00
VC0620	H	E	N	-	-	-	17.02	20.29	-	-	21.8	1.2	21.16	0.09	13.02	0.07	2.61	0.02	0.00
VC0688	H	T	N	D	15021.10	23.97	-	-	9.94	16.55	18.0	1.1	18.65	0.09	11.00	0.07	2.03	0.01	0.58
VC0737	H	T	N	E	-	-	25.52	19.58	11.32	18.56	14.6	1.1	19.33	0.12	12.72	0.06	2.13	0.04	0.34
VC0745	B	M	N	E	6.53	22.02	24.36	23.69	-	-	16.3	1.4	22.47	0.15	14.95	0.06	4.12	0.09	0.29
VC0745	H	E	?	-	8.99	18.26	-	-	-	-	8.8	1.1	18.31	0.23	11.99	0.06	2.94	0.05	0.00
VC0750	H	M	Y	E	5.25	19.47	22.58	20.49	-	-	18.2	1.5	19.84	0.15	11.95	0.06	3.90	0.02	0.15
VC0781	B	M	Y	E	4.52	21.94	15.52	22.43	-	-	13.2	1.3	21.93	0.17	14.98	0.07	4.08	0.07	0.17
VC0786	B	M	Y	E	10.25	23.32	32.13	23.68	-	-	27.8	3.0	23.20	0.15	14.84	0.11	3.84	0.24	0.18
VC0786	H	E	Y	-	-	-	16.20	19.58	-	-	15.6	1.4	19.66	0.17	12.21	0.06	3.28	0.01	0.00
VC0856	H	E	Y	-	-	-	14.83	18.98	-	-	14.3	1.2	18.93	0.15	11.27	0.06	2.76	0.04	0.00
VC0916	B	M	N	E	2.94	21.46	8.45	23.25	-	-	5.4	1.0	21.89	0.37	16.18	0.07	3.45	0.17	0.39
VC0951	B	M	N	E	6.63	22.34	25.85	23.24	-	-	21.1	1.6	22.59	0.13	14.46	0.07	4.00	0.08	0.26
VC0951	H	M	N	E	3.99	19.96	18.33	19.55	-	-	17.2	1.3	19.37	0.14	11.60	0.06	3.25	0.01	0.04
VC0965	B	M	B	E	0.92	21.65	21.67	23.42	-	-	23.0	1.4	23.72	0.10	15.54	0.06	3.45	0.03	0.01
VC0965	H	M	B	E	1.83	19.76	29.34	20.46	-	-	30.1	7.9	20.55	0.26	11.66	0.31	2.70	1.02	0.01
VC0975	H	M	N	E	6.79	20.46	49.74	21.28	-	-	48.5	3.3	21.20	0.09	11.06	0.09	3.03	0.14	0.04
VC1010	B	M	Y	E	8.55	21.89	24.85	22.53	-	-	21.9	1.4	22.09	0.10	13.89	0.07	3.13	0.05	0.18
VC1011	H	T	N	E	-	-	34.35	20.53	20.79	19.89	23.5	1.2	20.26	0.08	12.30	0.06	2.46	0.06	0.44
VC1036	B	M	Y	E	7.82	21.22	31.01	22.90	-	-	21.6	1.6	21.80	0.12	14.06	0.06	4.33	0.05	0.28
VC1036	H	M	Y	E	7.98	17.55	30.02	19.48	-	-	18.5	1.5	17.99	0.14	10.65	0.06	4.41	0.08	0.36
VC1047	H	D	N	-	23.93	17.40	-	-	-	-	25.9	1.7	17.56	0.12	8.71	0.06	7.42	0.21	1.00
VC1073	B	M	N	E	5.14	21.76	26.09	23.32	-	-	24.6	1.5	23.05	0.10	14.48	0.06	3.76	0.01	0.20
VC1073	H	M	N	E	2.77	17.87	12.30	18.58	-	-	10.8	1.1	18.15	0.20	11.41	0.06	3.79	0.06	0.11
VC1078	B	E	N	-	-	-	12.73	22.90	-	-	12.2	1.1	22.87	0.17	16.01	0.06	3.20	0.03	0.00
VC1078	H	E	N	-	-	-	11.44	20.15	-	-	11.7	1.1	20.20	0.17	13.37	0.06	2.74	0.01	0.00
VC1122	B	M	Y	E	9.05	22.08	28.88	23.71	-	-	16.6	1.4	22.04	0.15	15.00	0.06	4.13	0.11	0.43
VC1122	H	E	Y	-	12.37	18.67	-	-	-	-	11.8	1.0	18.75	0.16	11.99	0.06	3.48	0.03	0.00
VC1173	B	E	N	-	-	-	10.61	22.92	-	-	11.3	1.1	23.05	0.17	16.43	0.06	2.76	0.01	0.00
VC1173	H	E	N	-	-	-	11.77	19.79	-	-	12.1	1.1	19.89	0.17	13.20	0.06	2.84	0.01	0.00
VC1183	H	M	Y	E	4.48	17.89	23.71	19.65	-	-	15.3	1.6	18.44	0.19	11.14	0.06	5.54	0.06	0.22
VC1254	B	M	B	E	1.44	19.92	13.02	23.32	-	-	12.3	1.2	23.13	0.17	15.73	0.06	3.25	0.01	0.22
VC1254	H	M	B	E	0.93	16.97	13.02	19.47	-	-	12.2	1.4	19.33	0.23	12.07	0.06	3.39	0.05	0.05
VC1308	B	M	Y	E	6.87	22.49	19.25	24.11	-	-	11.1	1.2	22.31	0.20	15.75	0.07	3.77	0.04	0.44
VC1308	H	E	Y	E	7.84	18.84	-	-	-	-	7.5	1.0	18.78	0.26	12.73	0.06	3.13	0.10	0.00
VC1348	B	M	B	E	1.79	21.73	9.58	22.93	-	-	8.4	1.1	22.57	0.24	16.01	0.07	3.35	0.07	0.09
VC1348	H	M	B	E	1.19	17.77	8.26	18.99	-	-	7.7	1.0	18.78	0.25	12.42	0.06	3.19	0.10	0.06
VC1386	B	M	Y	E	16.57	23.73	52.87	25.27	-	-	34.7	4.0	24.00	0.17	14.82	0.10	4.15	0.34	0.35
VC1386	H	E	Y	-	19.79	20.17	-	-	-	-	20.90	1.2	20.35	0.10	12.07	0.06	3.08	0.01	0.00
VC1392	H	T	Y	E	-	-	44.82	20.31	16.76	19.22	22.8	1.2	19.99	0.09	12.04	0.07	2.01	0.01	0.41
VC1453	B	M	N	E	4.79	21.82	20.40	22.97	-	-	19.1	1.4	22.69	0.12	14.46	0.07	3.62	0.05	0.18
VC1453	H	M	N	E	3.07	18.28	10.86	18.60	-	-	10.1	1.1	18.31	0.19	11.58	0.07	3.15	0.07	0.10

Table 4. continued.

Galaxy	Filter	dec	Nuc	Bdec	Bulge		Disk exp		Outer exp		r_e	±	μ_e	±	M_T	±	C_{31}	±	B/T
					r_{ebf} arcsec	μ_{ebf} mag/□"	r_{edf} arcsec	μ_{edf} mag/□"	r_{eout} arcsec	μ_{eout} mag/□"	arcsec		mag/□"		mag				
(1)	(2)	(3)	(4)	(5)	(6)	(7)	(8)	(9)	(10)	(11)	(12)	(13)	(14)	(15)	(16)	(17)	(18)	(19)	(20)
VC1491	B	M	N	E	7.78	22.23	28.10	24.77	-	-	13.3	1.3	22.46	0.17	15.26	0.07	4.48	0.11	0.41
VC1491	H	M	N	E	7.23	18.48	36.41	21.70	-	-	15.1	5.1	19.13	0.55	11.64	0.20	5.75	1.77	0.46
VC1499	B	M	N	E	4.92	20.51	12.67	23.59	-	-	7.4	1.1	21.26	0.26	15.18	0.07	3.24	0.06	0.64
VC1499	H	E	N	-	7.21	18.39	-	-	-	-	7.7	1.0	18.47	0.25	12.57	0.07	2.74	0.04	0.00
VC1514	H	E	?	-	-	-	24.37	19.99	-	-	28.1	1.5	20.55	0.09	12.19	0.06	2.88	0.03	0.00
VC1528	H	M	N	E	2.74	17.01	10.06	18.60	-	-	7.9	1.1	17.83	0.25	11.45	0.07	3.56	0.14	0.18
VC1549	H	M	Y	E	4.61	18.27	14.25	19.26	-	-	11.6	1.1	18.61	0.18	11.44	0.06	3.47	0.01	0.20
VC1684	B	M	B	E	1.95	22.02	17.39	22.58	-	-	20.3	1.5	22.74	0.13	15.46	0.06	3.19	0.07	0.03
VC1684	H	M	B	E	2.08	21.08	19.76	19.82	-	-	20.6	1.1	19.89	0.09	12.64	0.06	2.68	0.00	0.01
VC1695	H	M	N	E	4.95	18.28	19.00	20.29	-	-	13.7	1.2	19.25	0.16	11.74	0.07	3.65	0.02	0.21
VC1834	H	T	Y	E	-	-	17.21	17.57	12.16	16.46	16.7	1.2	17.67	0.12	10.05	0.07	3.12	0.01	0.77
VC1895	H	M	N	E	7.13	18.94	19.89	20.01	-	-	13.8	1.2	18.86	0.14	12.11	0.08	3.89	0.20	0.24
VC1910	B	M	N	E	4.55	21.92	14.20	22.32	-	-	13.2	1.1	22.03	0.15	14.56	0.07	3.07	0.01	0.12
VC1947	H	E	Y	-	-	-	8.15	17.54	-	-	9.2	1.1	17.69	0.22	11.13	0.07	3.05	0.05	0.00
VC2042	H	E	Y	-	-	-	21.20	20.63	-	-	22.2	1.1	20.79	0.09	12.13	0.06	2.73	0.01	0.00
VC2050	H	E	N	-	-	-	11.64	19.00	-	-	13.1	1.1	19.28	0.15	12.37	0.06	2.85	0.02	0.00
2MASSX	H	D	N	-	4.19	17.01	-	-	-	-	5.2	1.1	17.47	0.40	12.10	0.06	5.90	0.02	1.00
CCC045	H	D	N	-	4.30	16.13	-	-	-	-	4.5	1.1	16.29	0.46	11.10	0.06	6.23	0.71	1.00
CCC059	H	M	N	E	0.57	18.17	4.27	19.97	-	-	4.1	1.1	19.81	0.47	15.00	0.10	3.38	0.21	0.10
CCC094	H	M	N	E	2.76	18.59	12.75	19.95	-	-	11.3	1.1	19.60	0.18	12.50	0.06	3.65	0.07	0.14
CCC095	H	M	N	D	2.62	14.69	25.07	19.33	-	-	11.6	1.2	17.02	0.19	10.16	0.06	8.42	0.37	1.00
CCC096	H	M	Y	E	8.20	17.37	17.97	18.67	-	-	12.0	1.1	17.14	0.17	10.54	0.07	3.65	0.03	0.46
CCC104	H	E	N	-	-	-	3.80	19.59	-	-	3.9	1.0	19.61	0.53	14.78	0.06	2.81	0.17	0.00
CCC113	H	M	N	E	1.44	17.61	4.36	18.73	-	-	3.4	1.0	17.93	0.60	13.42	0.07	3.35	0.35	0.25
CCC119	H	M	N	E	2.68	15.71	11.48	18.45	-	-	5.8	1.1	16.44	0.34	10.75	0.06	3.95	0.16	0.46
CCC122	H	M	N	E	2.49	14.43	20.01	17.91	-	-	8.1	1.2	15.38	0.28	9.59	0.07	7.24	0.38	0.34
CCC125	H	E	N	-	-	-	7.59	19.72	-	-	8.0	1.0	19.85	0.25	13.56	0.06	2.62	0.04	0.00
CCC136	H	M	N	E	0.88	16.07	3.89	17.84	-	-	3.0	1.0	17.04	0.70	12.79	0.07	3.84	0.58	0.21
CCC142	H	E	N	-	-	-	3.81	19.36	-	-	3.5	1.0	19.16	0.58	14.62	0.06	2.18	0.02	0.00
CCC150	H	E	N	-	-	-	4.21	20.01	-	-	4.2	1.0	20.05	0.48	15.16	0.06	3.11	0.23	0.00
CCC153	H	T	Y	E	-	-	4.80	19.12	3.06	18.05	3.8	1.0	18.88	0.52	14.53	0.07	2.63	0.12	0.67
CCC157	H	E	N	-	-	-	5.87	20.44	-	-	5.8	1.0	20.39	0.34	15.17	0.07	2.70	0.05	0.00
CCC205	H	M	N	E	1.51	16.02	7.90	18.67	-	-	4.6	1.1	17.08	0.46	11.96	0.06	5.28	0.72	0.32
CCC216	H	E	N	-	-	-	7.68	20.83	-	-	7.0	1.1	20.57	0.29	14.77	0.06	2.76	0.06	0.00
CCC222	H	M	N	E	1.41	18.01	8.90	18.88	-	-	9.3	1.1	18.84	0.22	12.20	0.06	3.22	0.04	0.06
CCC226	H	T	?	D	24.03	17.49	-	-	10.49	15.64	9.1	1.2	15.89	0.25	10.03	0.07	5.14	0.19	0.90
CEG050	H	M	N	E	1.18	19.13	3.38	19.27	-	-	3.1	1.0	18.96	0.67	14.63	0.07	3.10	0.27	0.11
97073	B	T	?	E	-	-	15.68	22.74	5.67	19.92	10.3	1.1	22.46	0.18	15.66	0.07	1.98	0.02	0.68
97073	H	E	?	-	-	-	10.04	19.87	-	-	10.4	1.0	19.94	0.19	13.19	0.06	2.74	0.02	0.00
97087	B	E	?	-	-	-	15.19	20.05	-	-	26.1	1.2	21.37	0.07	14.31	0.07	1.87	0.01	0.00
97087	H	E	?	-	-	-	12.59	16.72	-	-	14.4	1.2	16.98	0.15	11.01	0.07	3.45	-	0.00
IZW018	H	E	?	-	-	-	2.02	19.39	-	-	2.0	1.0	19.40	0.99	16.06	0.10	2.84	-	0.00

H-band data for 818 galaxies. These include all galaxies brighter than $m_p = 15.7$ in the Coma region, corresponding to $M_p < -19.2$ ($\mu = 34.9$) and 94% of galaxies brighter than $m_p = 14.0$ in the Virgo cluster, corresponding to $M_p < -17.2$ ($\mu = 31.2$), thus the observations of giant galaxies are complete. Considering only the Virgo cluster, we also covered 30% of galaxies in the interval $14.0 < m_p < 16.0$ corresponding to $-17.2 < M_p < -15.2$, thus to the transition region between giant and dwarf galaxies (see Sandage et al. 1985). The completenes in the same magnitude range increases from 30 to 47% if one considers the ISO sample only. The studied sample is representative of all Hubble types, including dE and Im, and spans 4 orders of magnitude in luminosity.

We model the surface brightness profiles of the studied galaxies with either a de Vaucouleurs $r^{1/4}$ law (D), an exponential law (E), a combination of the two (M), or with a profile that is truncated at the periphery (T). Using the fitted quantities we find that:

1) Less than 50% of the giant elliptical galaxies have pure D profiles;

The majority of giant galaxies (E to Sb) is best represented by a M profile. Scd-BCD galaxies have pure exponential profiles;

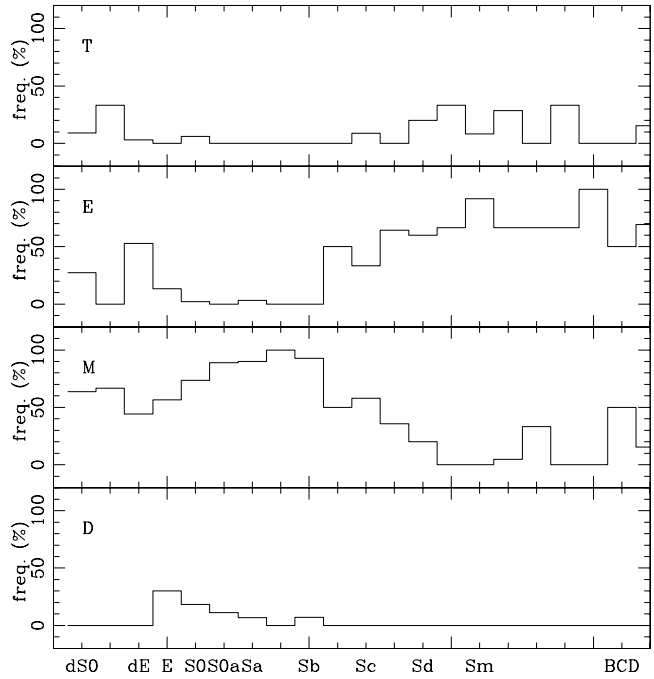

Fig. 5. The fraction of pure de Vaucouleurs, mixed, pure exponential and truncated profiles along the Hubble sequence for galaxies in the Virgo cluster.

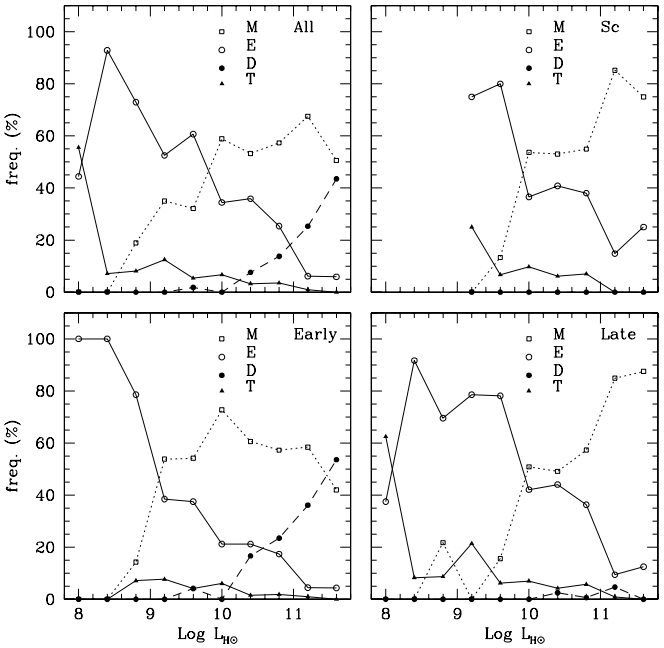

Fig. 6. The fraction of pure de Vaucouleurs, mixed, exponential and truncated profiles as a function of the NIR luminosity among all galaxies (top-left), among the Sbc-Sd (top-right), among early types (dE-E-S0a) (bottom-left) and among spirals (Sa-BCD) (bottom-right). The completeness levels of 100% and 50% for the Virgo cluster, computed assuming an average $B-H=3$ mag, are at 9.4 and 8.6 Log $L_{\mathrm{H}_\odot}$ respectively.

2) Most dwarf galaxies (independently from their detailed morphological type) follow exponential profiles or truncated decompositions;

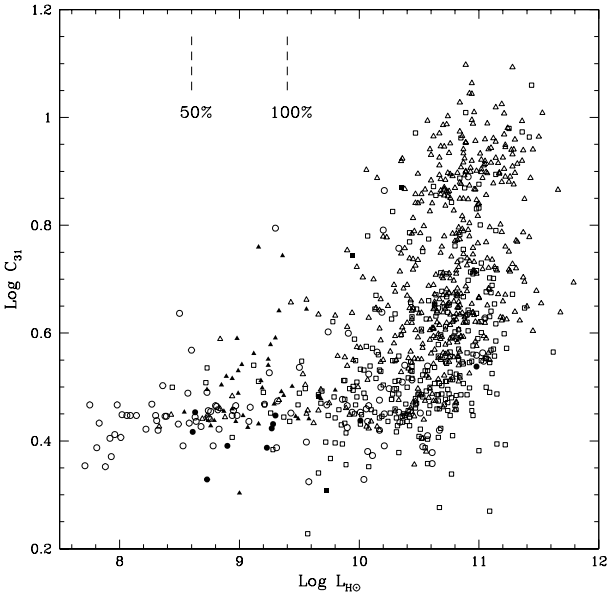

Fig. 7. The dependence of C_{31} on luminosity. Points are coded in three classes of Hubble type (dE-S0a = triangles; Sa-Scd = squares; Sd-BCD = circles). Measurements reported in this paper are given with filled symbols. Open symbols are from Paper V. Two completeness levels for the Virgo cluster, computed assuming an average $B-H=3$ mag, are indicated with dashed lines.

3) The type of decomposition is a strong function of the total H band luminosity ($10^8 < L_{\mathrm{H}} < 10^{11.5}\ L_\odot$), irrespective of the galaxy Hubble classification: the fraction of pure exponential profiles decreases with increasing luminosity, while that of M ones increases with luminosity. Truncated profiles are characteristic of the lowest luminosity galaxies. Pure D profiles are absent at low luminosities $L_{\mathrm{H}} < 10^{10}\ L_\odot$ and become dominant above $10^{11}\ L_\odot$;

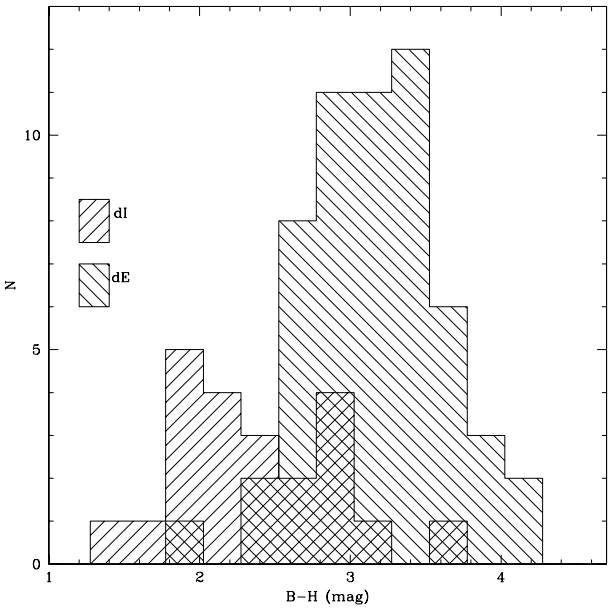

Fig. 8. The distribution of dE/dS0 and dI in bins of $B-H$.

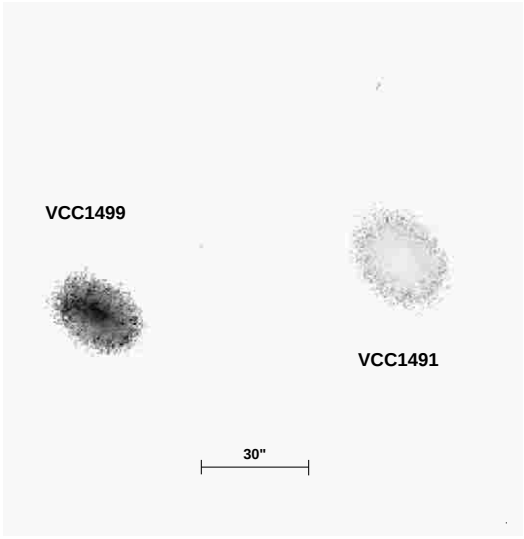

Fig. 9. $B-H$ color map of VCC1491-1499 (white = red, black = blue). Grey levels span from $B-H=2.35$ (darkest) to $B-H=3.75$. North is up, East to the left.

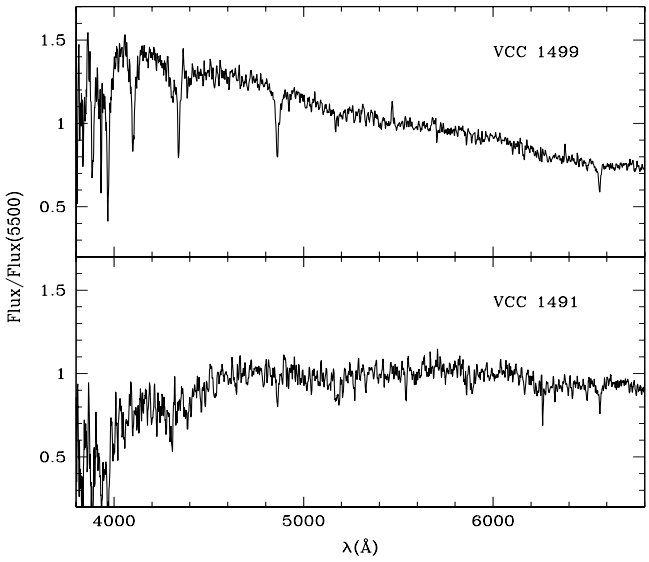

Fig. 10. Long-slit spectra of VCC1491-1499. The flux is normalized at 5500 Å.

4) The light concentration index C_{31} (presence of central cusps and extended outer haloes) is a strong non-linear function of the total luminosity, irrespective of the Hubble classification: dwarf systems have low C_{31}, typical of exponential disks; high C_{31}, characteristic of conspicuous bulges, are found only at the highest luminosities. There exist however a class of bulge-less, high luminosity galaxies. These are giant Sc's;
5) dE galaxies have mildly redder colors and higher C_{31} than dIs. The only subclass of early-type dwarfs having structural parameters indistinguishable from those of late-type dwarfs seems to be that of dE-pec, which therefore represents the possible missing link between dEs and dIs. This is supported by the evidence of post-starburst activity found in the dE-pec VCC1499.
The results summarized in points 1) through 4) should not suffer from selection biases since at low-luminosities, where our sample is severely incomplete, we observed primarily the highest surface brightness galaxies. Thus a bias, if any is present, should select in favour of high C_{31} galaxies with D or M profiles, because at comparable luminosities these objects have higher central surface brightness than those with low C_{31} and E or T profiles.
Summarizing, points 1–4 indicate that the frequency of occurrence of relevant cusps and extendend luminous haloes, absent among low-mass galaxies, increases significantly with increasing mass. This is consistent with the monolithic collapse scenario (Sandage 1986) provided that the collapse efficiency scales with mass (Gavazzi & Scodeggio 1996). If, otherwise, merging is invoked as the mechanism for building galaxies of increasing mass, a problem arises: while extended haloes are naturally produced as remnants of mergers between stellar disks, central high-brightness cusps require that the mergers occur in the presence of a gaseous phase (Hernquist et al. 1993). If this were the case, however, cusps (bulges) would be composed of younger stellar populations than it is generally observed.

Acknowledgements. We thank C. Bonfanti for the reduction and analysis of OHP spectra of two galaxies

References

Binggeli, B., Sandage, A., & Tammann, G. A. 1985, AJ, 90, 1681
Boselli, A., Tuffs, R., Gavazzi, G., Hippelein, H., & Pierini, D. 1997, A&AS, 121, 507 (B97)
Boselli, A., Gavazzi, G., Franzetti, P., Pierini, D., & Scodeggio, M. 2000, A&AS, 142, 73, Paper IV
Busko, I. 1996, Proceedings of the Fifth Astronomical Data Analysis Software and Systems Conference, Tucson, PASP Conf. Ser. 101, ed. G. H. Jacoby, & J. Barnes, 139
de Vaucouleurs, G. 1948, Ann. Astrophys., 11, 247
de Vaucouleurs, G. 1977, in Evolution of Galaxies and Stellar Populations, ed. R. Larson, & B. Tinsley (New Haven: Yale University Observatory), 43
Djorgovski, S., & Davis, M. 1987, ApJ, 313, 59
Dressler, A., Lynden-Bell, D., Burstein, D., et al. 1987, ApJ, 313, 42
Gavazzi, G., Pierini, D., Boselli, A., & Tuffs, R. 1996a, A&AS, 120, 489, Paper I
Gavazzi, G., Pierini, D., Baffa, C., et al. 1996b, A&AS, 120, 521, Paper II
Gavazzi, G., Pierini, D., & Boselli, A. 1996c, A&A, 312, 397
Gavazzi, G., & Scodeggio, M. 1996, A&A, 312, L29
Gavazzi, G., Boselli, A., Scodeggio, M., Belsole, E., & Pierini, D. 1999, MNRAS, 304, 595

Gavazzi, G., Franzetti, P., Scodeggio, M., et al. 2000a, A&AS, 142, 65, Paper III
Gavazzi, G., Franzetti, P., Scodeggio, M., Boselli, A., & Pierini, D. 2000b, A&A, 361, 863, Paper V
Hernquist, L., Spergel, D., & Heyl, J. 1993, ApJ, 416, 415
Hunt, L., Lisi, F., Testi, L., et al. 1996, A&AS, 115, 181
Hunt, L., Mannucci, F., Testi, L., et al. 1998, AJ, 115, 2594
James, P. 1991, MNRAS, 250, 544
James, P. 1994, MNRAS, 269, 176
Jedrzejewski, R. 1987, MNRAS, 226, 747
Jerjen, A., & Dressler, A. 1997, A&AS, 124, 1
Kauffmann, G., & Charlot, S. 1998, MNRAS, 294, 705
Kauffmann, G., & White, S. D. M. 1993, MNRAS, 261, 921
Kormendy, J., & Djorgovski, S. 1989, ARA&A, 27, 235
Larson, R. B. 1975, MNRAS, 173, 671
Lemaitre, G., Kohler, D., Lacroix, D., Meunier, J., & Vin, A. 1990, A&A, 228, 546
Lisi, F., Baffa, C., & Hunt, L. K. 1993, SPIE, 1495, 594
Lisi, F., Baffa, C., Bilotti, V., et al. 1996, PASP, 108, 364
Persson, S., Murphy, D., Krzeminski, W., Roth, M., & Rieke, M. 1998, AJ, 116, 2475
Poggianti, B., & Barbaro, G. 1996, A&A, 314, 379
Sandage, A., Binggeli, B., & Tammann, G. 1985, AJ, 90, 1759
Sandage, A. 1986, A&A, 161, 89
Sung, E., Han, C., Ryden, B., Chun, M., & Kim, H. 1998, ApJ, 499, 140
Tully, B., & Fisher, R. 1977, A&A, 54, 661
Whitmore, B. C. 1984, ApJ, 278, 61
Zwicky, F., Herzog, E., Karpowicz, M., Kowal, C., & Wild, P. 1961–1968, Catalogue of Galaxies and Clusters of Galaxies, vol. 6, Pasadena, C.I.T.